Investigating gamma-tubulin's function in spindle microtubule pairing using yeast-optimized TurboID

Colten Peters

Master of Science

Department of Biology

McGill University

Montreal, Quebec, Canada

October 2024

A thesis submitted to McGill University in partial fulfillment of the requirements of the degree of Master of Science

Acknowledgements

I would like to begin by expressing my utmost and sincere gratitude to the entire Vogel lab, current and past, who have helped me grow as both a scientist and a person. First, I would like to offer my utmost thanks and gratitude to Dr. Jackie Vogel, whose guidance and supervision have shaped and refined my ability to interact and engage with science. Her mentorship has taught me how to be both rigorous and think outside of the box (especially the latter). Thank you as well to Jackie for her generous financial support through the Canadian Institutes of Health Research project grants which funded my research. Also, thank you to my supervisory committee, Dr. Gary Brouhard, Dr. Anthony Mittermaier, and Dr. Alba Guarne.

I would like to thank Dr. Ziad El-Hajj, who is both a great colleague and a superb friend, for his utmost support in both science and life. I would like to thank all of the Vogel lab graduate students, including: Shannon Sim, for her unwavering kindness; Katherine Morelli, for her classification debates; Khalid Al'Naemi, for his rhetorical "questions"; Sean Moore, for his easygoing nature (and quote log); Tanaka Mutsayi, for her valuable input; and Yiran Fan, for her kind spirit.

I would also like to thank all of the Vogel lab undergraduate students who I have worked with. Thank you to Maddy Willis, Angela Zhao, Emma Rousseau, Nancy Krug, Stephanie Skaltizsky, Roan Blakely, Soraya Ghassemlou, and Genevieve Quinn. Special thanks to Emma, who played a pivotal role in initiating the use of BioID and establishing the bioinformatic pipeline. Also, thank you to the undergraduates who have dissected yeast for me throughout my degree, including Julien Turk, Mavis Lee, Angie Cho, and Jou Zouein.

Next, I thank the Oeffinger lab for graciously allowing me to become a semi-member of their lab, including full use of their equipment and many reagents, and my own bench space. Their support and collaboration played a pivotal role in my degree. First, my utmost thanks to Dr. Marlene Oeffinger for her help throughout this degree. I would also like to express my absolute gratitude to Dr. Christian Trahan, who has provided significant scientific support and played a pivotal role in my progression. Thank you as well to Lisbeth-Carolina Aguilar for her help and kind-

hearted nature. Lastly, thank you to Sonny (Pudchalaluck) Panichnantakul, who was an incredible colleague and has become a good friend.

Finally, I wish to take this opportunity to thank all of my family for their endless love and support. I would not have finished this degree without them. Most importantly, I would like to express my deepest appreciation for my future wife, Nhu Y (Emily) Truong, who moved with me to Montreal while I completed this degree. She has provided endless support, love, and guidance—both scientific and personal—which has not only enabled me to finish this degree but has truly shaped me into a better person. Anh yêu em, Emily.

Table of Contents

List of Tables

Chapter 3

Chapter 4

List of Figures

Chapter 1

Chapter 3

Figure 3.14. The Y445D mutation inhibits Cin8 interactions with γTuRC and kinetochore proteins.

List of Abbreviations

AID	Auxin-inducible degron
aMT	Astral Microtubule
BioID	Biotin Identification
CDK	Cyclin-Dependent Kinase
CT	Carboxyl Terminus
HIS	Histidine
ipMT	Interpolar-Microtubule
kMT	Kinetochore-Microtubule
MAP	Microtubule-Associated Protein
MS	Mass Spectrometry
MT	Microtubule
MTOC	Microtubule-Organizing Centre
NMR	Nuclear Magnetic Resonance
SAC	Spindle Assembly Checkpoint
SIM	Structured Illumination Microscopy
SPB	Spindle Pole Body
URA	Uracil
WT	Wild-Type
γTuRC	γ-Tubulin Ring Complex
γTuSC	γ-Tubulin Small Complex

Author Contribution

All data shown in Chapter 3 is the result of my work as an M.Sc. student in the Vogel lab. Figure 1.1 in Chapter 1 was created by my supervisor and edited by me. Figure 1.2 in Chapter was created by me in ChimeraX using published Monte Carlo structures from Harris et al. (2017) and the γTuRC structure PDB:5FLZ by Kollman et al. (2015). All figures in Chapter 2 were created by me. Figure 2.2 in Chapter 2 was created by me in ChimeraX using the γTuRC structure PDB:5FLZ by Kollman et al. (2015). ImageJ was used to quantify signal of SDS-PAGE separated proteins on western blots in Chapter 2 figures 2.3 and 2.7. Dot plots in Chapter 2 figures 2.6, 2.10 and 2.11, and the scatter plot in Chapter 2 figure 2.12 was created using the ProHits-Viz online analysis suite. Volcano plots in Chapter 2 figures 2.5, 2.8, and 2.9 were created using the online VolcaNoseR Shiny app. The clustered proteins in Chapter 2 figure 2.13 was created using Cytoscape.

The research plan for the project was developed by Jackie Vogel, with assistance from Marlene Oeffinger and Christian Trahan. Unless otherwise indicated, all yeast strains and plasmids were made by me. Primer design was done by me with support from Ziad El-Hajj. Yeast dissection was conducted by Julien Turk, Mavis Lee, Angie Cho, and Joe Zouein. Emma Rousseau and I collaborated equally on the initial setup of the bioinformatic pipeline. Proteomic samples were processed and injected on an Orbitrap Fusion Mass Spectrometer by the proteomics facility of the Institut de recherches cliniques de Montréal (IRCM). MS data was analyzed using MaxQuant and Perseus. Shannon Sim translated the English abstract to French. I wrote all chapters of my thesis, and my supervisor edited all chapters of my thesis.

Abstract

Cell division relies on the accurate partitioning of chromosomes, driven by the mitotic spindle composed of microtubules (MTs), MT-associated proteins (MAPs), and MT-organizing centers (MTOCs). MTs are nucleated by γ-tubulin ring complexes (γTuRCs) at MTOCs, which serve as a template for MT formation. MTs are polarized polymers where the minus-end remains anchored by the γTuRC template while the plus-end alternates between growth and shrinkage. While γ-tubulin is known for its role in MT assembly, research from the Vogel lab has revealed it also has functions in specifying how proteins interact with MTs. Previous work identified a conserved phosphorylated residue in the γ-tubulin C-terminus (γCT), Tyrosine 445 (Y445), that appears to act in assembly of interpolar-MTs (ipMTs) at the spindle midzone. The phospho-mimetic Y445D mutation disrupts the function of Cin8, a kinesin-5 motor protein, reducing its localization to ipMT overlaps and increasing its presence at the minus-ends of MTs nucleated by γTuRCs at the spindle pole. This is correlated with a destabilization of the nascent bipolar spindle. The precise role of the γCT in ipMT assembly remains unclear, largely due to the lack of identified interactors beyond other MTOC components. I hypothesized that interactors involved in γ-tubulin's additional functions may bind with low affinity or transiently, evading detection by traditional methods which require stable interactions that can endure harsh lysis and purification conditions. To address this, I adapted the BioID proximity labeling method, traditionally used in mammalian cells, to detect potential γ-tubulin interactions in yeast. However, there are several challenges for BioID's application in yeast. The first is the tough cell wall, which can be overcome using cryogrinding. The second is the high background signal from native biotinylated enzymes. To overcome this, I used an auxin-inducible degron system to degrade the yeast biotin ligase Bpl1 and reduce endogenous biotinylation. Finally, I employed mild denaturation conditions to preserve transient interactions and native protein complexes. Using this optimized method, I aimed to identify candidate proteins involved in the γCT mechanism influencing ipMT assembly and how the Y445D mutation alters Cin8 interactions. I screened for interactors of Spc97, a stable component of the γTuRC, and Cin8. The Spc97 screen successfully recapitulated several high-confidence interactions reported in the literature, as well as detected numerous proteins involved in ipMT assembly and novel interaction candidates. The Cin8 screen identified interactions with

all components of the γTuRC, including the nuclear receptor Spc110. Notably, this signal was significantly reduced in the γtub-Y445D mutant background, further supporting a role for γ-tubulin in mediating Cin8's interactions at the minus-ends of MTs. This study lays the groundwork for generating valuable hypotheses for future experiments focused on investigating the candidate proteins and elucidating the molecular mechanisms by which γ-tubulin regulates Cin8 and ipMT assembly, while also showcasing the broader potential of combining BioID with the yeast model system to map complex protein interaction networks.

Abrégé

La division cellulaire dépend de la séparation précise des chromosomes. Ce processus est assuré par le fuseau mitotique, composé de microtubules (MTs), de protéines associées aux MTs (MAPs) et de centres organisateurs de MTs (MTOCs). Les MTs sont nucléés par des complexes en anneau de la tubuline-γ (γTuRCs), situés aux MTOCs, qui servent de gabarits pour la formation des MTs. Les MTs sont des polymères polarisés avec une extrémité moins ancrée par le γTuRC et une extrémité plus qui alterne entre croissance et décroissance. La tubuline-γ est connue principalement pour son rôle dans la nucléation des MTs, mais les recherches du laboratoire Vogel ont révélé qu'elle contribue aussi au contrôle des interactions entre les protéines et les MTs. Des travaux antérieurs ont identifié un site phosphorylé conservé dans l'extrémité c-terminale de la tubuline-γ (γCT), la tyrosine 445 (Y445), qui semble contribuer à l'assemblage des MTs interpolaires (ipMTs) de la zone médiane du fuseau. La mutation phospho-mimétique Y445D perturbe la fonction de Cin8, une protéine motrice de la famille kinésine-5. Cette mutation réduit la présence de Cin8 aux chevauchements des ipMTs et augmente sa présence aux extrémités moins des MTs nucléés par les γTuRCs aux pôles mitotiques. Ces changements sont corrélés avec une augmentation de l'instabilité des fuseaux naissants. Le rôle précis que joue l'γCT dans la formation des ipMTs demeure incertain, en raison notamment du manque d'interacteurs connus autres que les composantes des MTOCs. J'ai hypothétisé que des interacteurs qui contribuent aux autres fonctions de la tubuline-γ forment peut-être des associations de moins grande affinité ou de moins longue durée. Les méthodes de détections traditionnelles ne pouvant détecter que les interactions stables qui peuvent survivre à des conditions de purification intenses, ces interactions évitent peut-être la détection. Pour répondre à cette question, j'ai adapté la méthode de marquage de proximité BioID, traditionnellement utilisée dans les cellules de mammifères, afin de détecter des interactions potentielles avec la tubuline-γ dans la levure. Toutefois, l'application de la BioID dans la levure présente plusieurs défis. La première est la paroi cellulaire, qui peut être surmontée à l'aide du cryobroyage. La deuxième est le signal de fond élevé provenant d'enzymes biotinylées natives. Pour surmonter cela, j'ai utilisé un procédé de dégradation inductible par l'auxine pour dégrader la biotine ligase de levure Bpl1 afin de réduire la biotinylation endogène. Finalement, j'ai utilisé des conditions de dénaturation douces afin de

conserver les interactions transitoires et les complexes protéiques natifs. Avec cette méthode optimisée, j'ai cherché à identifier des protéines candidates impliquées dans le mécanisme par lequel l'γCT influence la formation des ipMTs et dans l'altération des interactions de Cin8 dans le mutant Y445D. J'ai cherché des protéines interagissant avec Spc97, une composante stable du γTuRC, et Cin8. Le criblage de Spc97 a réussi à reproduire plusieurs interactions rapportées dans la littérature et à détecter des interactions avec plusieurs protéines impliquées dans la formation des ipMTs et des nouveaux interacteurs potentiels. Le criblage de Cin8 a identifié des interactions avec toutes les composantes du γTuRC, dont le récepteur nucléaire Spc110. Notamment, ce signal est considérablement réduit dans le fond génétique γtub-Y445D, ce qui renforce l'idée que la tubuline-γ joue un rôle dans le contrôle des interactions de Cin8 aux extrémités moins des MTs. Cette étude pose les bases pour la génération d'hypothèses utiles pour des travaux futurs axés sur l'étude des protéines candidates et l'élucidations des mécanismes moléculaires par lesquels la tubuline-γ régule Cin8 et l'assemblage des ipMTs, tout en mettant en valeur le potentiel de la combinaison de la méthode BioID avec la levure pour cartographier des réseaux complexes d'interactions protéiques.

INTRODUCTION

Rationale

Cell division relies on the accurate partitioning of chromosomes, a process driven by the mitotic spindle, which is composed of microtubules (MTs), MT-associated proteins (MAPs), and MT-organizing centers (MTOCs). MTs are nucleated by γ-tubulin ring complexes (γTuRCs) at MTOCs, which act as a template for MT formation. MTs are polarized polymers with a minus-end anchored by the γTuRC, and a plus-end which undergoes dynamic cycles of growth and shrinkage. Although γ-tubulin is best known for its role in MT nucleation, research from the Vogel lab has shown it also plays a role in specifying how proteins interact with MTs.

Previous work in the Vogel lab identified a conserved phosphorylated residue in the unstructured C-terminus of γ-tubulin (γCT), Tyrosine 445 (Y445; Shulist et al., 2017; Vogel et al., 2001; Vogel & Snyder, 2000), which appears to be involved in the assembly of interpolar microtubules (ipMTs) at the spindle midzone. The phospho-mimetic Y445D mutation disrupts the function of Cin8, a kinesin-5 motor protein, reducing its localization to ipMT overlaps and increasing its accumulation at the minus-ends of MTs nucleated by γTuRCs at the spindle pole (Sim et al., 2024). This mislocalization also correlates with destabilization of the nascent bipolar spindle (Sim et al., 2024).

Since γ-tubulin remains associated with the MT minus-end throughout mitosis in budding yeast, the mechanism by which the γCT Y445D mutation influences Cin8 localization likely involves other interacting proteins. However, this mechanism remains poorly understood, as proteins known to interact with γ-tubulin are largely restricted to MTOC components. Given that the γCT is a disordered region, I hypothesized that the proteins involved in this mechanism may interact with γ-tubulin transiently or with low affinity—properties common to interactions involving disordered regions. These transient interactions are difficult to detect using traditional methods, which typically rely on stable interactions that can withstand harsh lysis and purification conditions.

Objectives

This work has two primary goals. The first is to adapt and optimize a yeast TurboID method for detecting proteins with transient or low affinity interactions with the γTuRC. The second is to apply this optimized method to identify candidate proteins in wild-type (WT) cells and the Y445D γ-tubulin mutant, which may play a role in the γCT-mediated mechanism affecting ipMT assembly and Cin8 function.

CHAPTER 1 – LITERATURE REVIEW

1.1. Overview of the mitotic spindle in the eukaryotic cell cycle.

The cell cycle in eukaryotic cells is a highly regulated sequence of events leading to cell growth, DNA replication, and cell division. It is traditionally divided into four main phases: G1 phase (gap 1), S phase (synthesis), G2 phase (gap 2), and M phase (mitosis). During this cycle, cells duplicate their genetic material and partition it equally between two daughter cells during mitosis. The mitotic spindle, a critical structure during mitosis, is a dynamic assembly composed of MTs, MT-nucleating proteins, and MAPs, which functions to accurately segregate duplicated chromosomes (Winey & Bloom, 2012).

1.1.1. The stages of mitosis are coupled to specific mitotic events.

Mitosis itself can be divided into four key stages: prophase, metaphase, anaphase, and telophase. Each stage is dependent on proper mitotic spindle function, beginning with spindle assembly during prophase, which is triggered by the phosphorylation of key substrates by cyclin-dependent kinase (CDK) complexes bound to specific cyclins. During prophase, duplicated centrosomes (or spindle pole bodies in yeast) migrate to opposite poles of the cell, facilitated by kinesin-5 motor proteins that crosslink pairs of intersecting MTs at short overlaps (Leary et al., 2019). These MT pairs, with one originating from each opposing spindle pole, serve as the precursors to the ipMTs, which become a stabilizing core at the spindle midzone during metaphase. This process is crucial for the initial establishment of the bipolar mitotic spindle and prepares the cell for chromosome alignment and segregation during subsequent stages of mitosis.

In metaphase, the precursor ipMTs mature with the recruitment of additional kinesin-5, which slides the antiparallel MTs apart to generate outward force. The kinesin-5 sliding forces contribute to both spindle stability and spindle elongation (Leary et al., 2019). However, these outward forces are counteracted by inward-directed tension from two primary sources: chromatid cohesin, which holds sister chromatids together, and kMTs, which attach to kinetochores on chromosomes and exert pulling forces during chromosome biorientation. The balance between these outward and inward forces ensures proper chromosome alignment at the metaphase plate, positioning them for segregation during anaphase, while also maintaining spindle integrity and preventing it from either collapsing or overextending (Dumont & Mitchison, 2009).

During anaphase, the spindle undergoes a dramatic transformation as the cohesin complexes that hold sister chromatids together are cleaved by separase, allowing the chromatids to separate. The kMTs begin to depolymerize, pulling the now-separated sister chromatids toward opposite ends of the cell. Simultaneously, ipMTs undergo polymerization and elongation, while motor proteins—primarily kinesin-5—slide the antiparallel ipMTs apart. This sliding pushes the spindle poles further apart, aiding in the efficient segregation of chromatids. The coordinated depolymerization of kMTs and the outward sliding of ipMTs ensure that each daughter cell receives an identical set of chromosomes.

In telophase, the separated chromosomes reach the spindle poles and begin to decondense, while the mitotic spindle initiates disassembly. Spindle disassembly actually begins earlier, in anaphase, when the Spindle Assembly Checkpoint (SAC) is satisfied, lifting its inhibitory signal on the anaphase promoting complex (Peters, 2006; Musacchio, 2015). The activation of anaphase promoting complex coordinates the degradation of key mitotic regulators, including B-type cyclins and proteins that maintain spindle stability, such as ipMT crosslinkers. This coordinated degradation continues through telophase, promoting the depolymerization of spindle MTs and the separation of the spindle poles, effectively signaling the end of mitosis. After spindle disassembly, cytokinesis occurs, during which the cell's cytoplasm is divided, physically separating the two daughter cells and completing the cell division cycle.

The precise progression of these mitotic stages, particularly those involving spindle dynamics, is tightly regulated by oscillating levels of cyclins and CDK activity (Kõivomägi et al., 2011). Cyclin-CDK complexes phosphorylate key proteins to control spindle assembly, MT dynamics, and chromosome segregation. This regulation ensures that the spindle is properly assembled and functional throughout mitosis. In tandem, checkpoint complexes, such as the SAC, monitor spindle dynamics and chromosome attachment, pausing the cell cycle if any errors, such as improper kinetochore-MT attachments, are detected. These mechanisms collectively safeguard the fidelity of mitosis, preventing chromosome mis segregation and ensuring accurate division.

These tightly regulated processes of spindle assembly and chromosome segregation during mitosis are conserved across eukaryotic organisms. To study these mechanisms in greater detail, model systems are invaluable, providing simplified yet informative contexts for understanding complex cellular dynamics.

1.1.2. A note on using budding yeast to investigate fundamental cellular processes.

The budding yeast *Saccharomyces cerevisiae* (*S. cerevisiae*) is a widely used and powerful model system for studying highly conserved eukaryotic cellular processes. Arguably, its greatest contribution lies in the discovery and characterization of the fundamental mechanisms that govern cell cycle timing, including the assembly and function of the mitotic spindle. The mitotic spindle in budding yeast is simple and highly stereotyped, comprising two spindle pole bodies (SPBs) and a small number of MTs, with components highly conserved across eukaryotic species (Kilmartin, 2014).

Unlike other eukaryotes, where MTs can be nucleated via chromatin-mediated or branching pathways, in budding yeast, MTs are exclusively nucleated from the SPBs (Roostalu & Surrey, 2017). Yeast MT nucleation is also simplified, relying solely on the three core components required for MT nucleation in all eukaryotes: γ-tubulin, Spc97/GCP2, and Spc98/GCP3 (Kollman et al., 2010, 2011, 2015). The yeast minimal nucleation system lacks the additional, non-essential proteins present in other organisms that provide regulatory or accessory functions (Roostalu & Surrey, 2017). Additionally, budding yeast expresses only a limited subset of the tubulin code,

expressing a smaller repertoire of tubulin isotypes, which undergo fewer post-translational modifications, further reducing the complexity of MT regulation compared to other eukaryotes (Janke, 2014).

Moreover, budding yeast is highly genetically tractable, enabling straightforward insertion and characterization of mutations through homologous recombination, making it easy to create strains with specific genetic alterations. This, combined with effective protocols for cell lysis and purification of native protein complexes, allows for efficient biochemical analysis and protein interaction studies. These features make budding yeast an excellent system for dissecting the fundamental mechanisms underlying MT organization and for investigating how γ-tubulin controls how proteins interact with MTs, including identifying transient or low-affinity interactions that may be involved in the mechanism.

In conclusion, budding yeast serves as an exceptional model for elucidating core processes in cell biology, providing a simplified yet highly informative system to study mechanisms of MT organization. Its genetic tractability and highly conserved cellular components make it ideal for exploring γ-tubulin's potential role in coordinating protein interactions with MTs, offering valuable insights into conserved eukaryotic processes.

1.2. A component list of the mitotic spindle.

Hundreds of proteins, regulated by kinases and phosphatases, work in coordination to drive the function of the mitotic spindle. However, the essential structural components of the spindle are MTs, MAPs, and MT nucleators (Winey & Bloom, 2012). Of these, the most abundant component is the MTs themselves, whose function is tightly regulated by MAPs and nucleating proteins. This section will provide an overview of these three key spindle components: MTs, MAPs, and the proteins that nucleate MTs.

1.2.1. Microtubules: highly dynamic and polarized polymers.

MTs are evolutionarily conserved polymers that form the structural framework of the mitotic spindle, facilitating the forces necessary for chromosome segregation during cell division. Composed of α/β-tubulin heterodimers, MTs assemble into linear protofilaments—typically 13—

that arrange around a hollow core (Brouhard & Rice, 2018). Each MT has a plus-end, which alternates between phases of growth and shrinkage, and a minus-end, which remains anchored to MTOCs in budding yeast. The tubulin dimers are oriented such that β-tubulin is exposed at the plus-end, where the MT is stabilized by the GTP-cap, and α-tubulin faces the minus-end (Gudimchuk & McIntosh, 2021).

All tubulins possess a GTP-binding domain, and both α-tubulin and β-tubulin bind GTP prior to their incorporation into the MT lattice (Nogales et al., 1998; Aldaz et al., 2005; Gudimchuk & McIntosh, 2021). However, only β-tubulin hydrolyzes GTP during the lifetime of the MT. When the rate of GTP-bound dimer addition fails to keep pace with GTP hydrolysis, leading to an excess of GDP-bound dimers, the stabilizing GTP-cap is lost (Hyman et al., 1992; Müller-Reichert et al., 1998; Tian et al., 1999). This loss triggers rapid MT disassembly, an event known as catastrophe. However, a shrinking MT can switch back to a growth phase, an event called a rescue. These alternating phases of catastrophe and rescue define the MT property known as dynamic instability, which is essential for the dynamic function of the mitotic spindle during cell division (Brouhard & Rice, 2018).

1.2.2. Microtubule-associated proteins.

MAPs in eukaryotic cells play pivotal roles in modulating MT dynamics and functions (Amos & Schlieper, 2005; Goodson & Jonasson, 2018; Bodakuntla et al., 2019). By decorating the MT lattice, MAPs regulate MT stability, facilitate interactions with other proteins, and bundle MTs into specialized arrays. They employ a wide range of mechanisms, binding either to the MT lattice or to the ends of MTs, and are broadly categorized into MT stabilizers/destabilizers, plus-end tracking proteins (+TIPs), and motor proteins that traverse along the lattice and crosslink adjacent MTs (Amos & Schlieper, 2005).

The activity of MAPs is finely regulated through cell cycle-specific post-translational modifications, which can occur on the MAPs themselves or on tubulin—the primary structural component and interaction interface of MTs (Janke, 2014). Many organisms express multiple tubulin isotypes, each possessing distinct physicochemical properties. The specific composition and ratio of these tubulin isotypes within the MT lattice can influence MAP binding affinities and

specificities. Furthermore, both α- and β-tubulins feature glutamate-rich, disordered carboxyl-terminal (CT) tails, known as E-hooks, which create a highly negatively charged interface crucial for MAP interactions (Nogales et al., 1998; Lakämper & Meyhöfer, 2005; Ramey et al., 2011; Scholey et al., 2014). Post-translational modifications targeting the CT domains can modify the charge distribution along the MT surface, significantly affecting MT-MAP interactions and, consequently, the dynamics of the cytoskeleton.

1.2.3. Microtubule nucleating proteins.

The assembly of MT polymers occurs in two distinct stages: an initial, rate-limiting nucleation phase followed by rapid elongation. Spontaneous nucleation of MTs from soluble GTP-bound α/β-tubulin heterodimers is inherently slow and energetically unfavorable under physiological conditions (Erickson & Pantaloni, 1981; Kuchnir Fygenson et al., 1995). This spontaneous process requires tubulin concentrations much higher than those typically found within cells, making it inefficient and unlikely to occur. To overcome this nucleation bottleneck, cells have evolved specialized mechanisms to spatially and temporally regulate MT nucleation, ensuring that MT assembly occurs precisely where and when it is needed.

The canonical nucleation mechanism involves the γTuRC, which is anchored at MTOCs such as centrosomes in animal cells or SPBs in yeast. The γTuRC presents a left-handed, 14-spoked helical template that mimics the MT lattice structure, providing a scaffold for the addition of α/β-tubulin dimers (Kollman et al., 2011). The essential core of this complex is the conserved γ-tubulin small complex (γTuSC), which constitutes the minimal unit necessary for MT nucleation.

Each γTuSC consists of two accessory proteins, Spc97 and Spc98, which form two interacting spokes within the γTuSC structure (Kollman et al., 2010, 2015). Each spoke binds a copy of γ-tubulin, positioning it in a way that templates the geometry of the growing MT. Within this complex, the γ-tubulins interact directly with the α-tubulin subunits of incoming α/β-tubulin dimers, forming longitudinal contacts that stabilize the nascent MT. Additionally, the γ-tubulins promote lateral interactions between adjacent tubulin dimers, facilitating the assembly of the MT lattice. This templating mechanism effectively lowers the energetic barrier for MT nucleation, allowing MTs to form efficiently under physiological conditions.

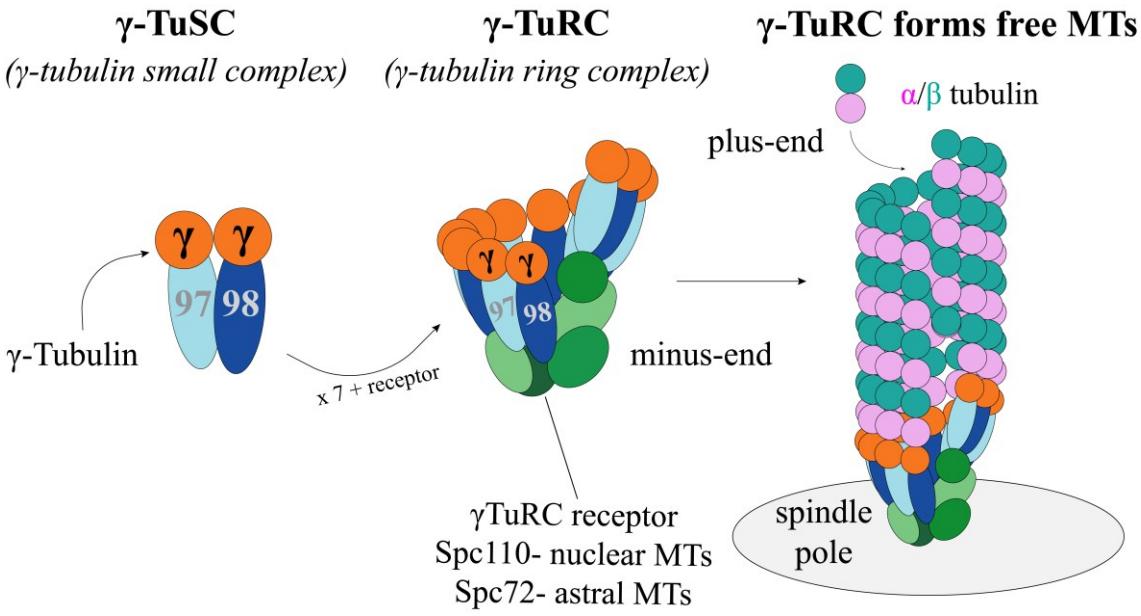

Figure 1.1. Microtubules are nucleated by γ-tubulin complexes. γ-Tubulin, Spc97, and Spc98 form γ-tubulin small complexes (γTuSCs). Seven γTuSCs oligomerize into ring complexes (γTuRCs) anchored to a spindle pole which act as templates to nucleate MTs. Figure by J. Vogel.

Notably, while many organisms possess additional γTuRC components that provide further regulation and specialization of MT nucleation, budding yeast contains only the essential γTuSC components: γ-tubulin, Spc97, and Spc98 (Roostalu & Surrey, 2017). This simplicity makes budding yeast an excellent model system for studying the fundamental mechanisms of MT dynamics without the complexity introduced by additional regulatory proteins.

1.3. The organization and specification of microtubules into functional arrays.

The precise spatial and temporal regulation of MT organization is fundamental to proper mitosis. MTs must be arranged into ordered and functional arrays to facilitate processes such as spindle positioning and chromosome segregation. MT organization begins with nucleation initiated by the γTuRC, which anchors their minus-ends to MTOCs, establishing the initial MT framework.

However, MTOCs alone are insufficient to form the distinct MT arrays required for specific cellular functions. MAPs are essential in this process, regulating the arrangement, stabilization, and interaction of MTs within the cellular context (Akhmanova & Steinmetz, 2015). By selectively binding to MTs, MAPs define and regulate the behavior of MT arrays, ensuring they function

according to the specific demands of the cell. Importantly, the formation and maintenance of these arrays are tightly coupled to the cell cycle, with kinases and phosphatases coordinating MAP activity to synchronize MT organization with key mitotic events. Through this dynamic regulation, MT arrays provide the structural foundation necessary for chromosome segregation and other critical processes during cell division.

1.3.1. The spindle pole body: the primary site for budding yeast microtubule nucleation.

MTOCs are the primary sites for MT nucleation and play a crucial role in controlling the orientation and organization of MTs into bundles. While some organisms can nucleate MTs from alternative locations, all MTs in budding yeast originate from one of two SPBs. Each SPB consists of three cylindrical layers—called plaques—embedded in the nuclear envelope: the inner plaque faces the nucleus, the central plaque aligns with the plane of the nuclear envelope, and the outer plaque faces the cytoplasm (Winey & Bloom, 2012).

Since yeast undergoes closed mitosis, where the nuclear envelope remains intact, the SPB separates two distinct classes of MTs: cytoplasmic MTs nucleated from the outer plaque and nuclear MTs nucleated from the inner plaque. These plaques serve as platforms for MT nucleation by anchoring receptor proteins—Spc72 in the cytoplasm and Spc110 in the nucleus—that bind γTuRCs. This arrangement allows the SPB to act as a scaffold that organizes polarized bundles of MTs within each cellular compartment.

Adjacent to the plaques is a specialized region of the nuclear envelope known as the half-bridge, which is essential for SPB duplication (Jaspersen & Winey, 2004). In the G1 phase, the half-bridge begins to elongate, and a SPB precursor forms at its distal end. This precursor matures into a fully functional SPB during S-phase, resulting in the duplication of the SPB once per cell cycle and yielding a pre-existing 'old' pole and a newly formed 'new' pole. Notably, during mitosis in unperturbed cells, the old pole is consistently inherited by the daughter cell, while the new pole remains in the mother cell.

1.3.2. Microtubule organization by microtubule-associated proteins.

In budding yeast, each MT is anchored at its minus-end to one of two SPBs. To fulfill specialized functions during mitosis, these MTs must be organized into distinct arrays—a process orchestrated by MAPs. In the cytoplasm, MT arrays interact with cortical elements, utilizing MT pushing and pulling forces to properly position and align the spindle. Within the nucleus, there are two primary MT arrays. The first consists of kMTs that dynamically grow and shrink to search for and attach to kinetochores. The second comprises ipMTs originating from both spindle poles, forming a core stabilizing bundle in the midzone. These ipMTs are pairs of antiparallel MTs, one from each opposing spindle pole, cross-linked by MAPs at overlapping regions. Through the action of MAPs, the cell directs the organization and function of these MT arrays, ensuring proper spindle dynamics and accurate chromosome segregation.

Each specialized MT array harbors a unique set of MAPs tailored to its specific mitotic role. For example, nuclear kMT arrays are enriched with proteins that modulate MT assembly and disassembly. Plus-end localized MT polymerases, such as Stu2 (the XMAP215 homolog), promote kMT assembly while counteracting the action of MT depolymerases like Kip3 (Amin et al., 2019). This balance allows kMTs to efficiently probe the three-dimensional cellular space and precisely locate kinetochores. In contrast, nuclear ipMTs stabilize the spindle by generating outward-directed forces to counterbalance the inward-directed forces from kMTs attached to kinetochores (Petry, 2016). To achieve this, crosslinking MAPs—such as kinesin-5 and the non-motor crosslinker Ase1/PRC1—are enriched at the overlaps of ipMTs (Leary et al., 2019; She et al., 2019), forming crosslinks that increase the rigidity and stiffness of each MT pair (Mickey & Howard, 1995).

MT organization varies not only between cellular compartments but also depending on the SPB from which they originate. For instance, the cytoplasmic bundles of astral MTs (aMTs) on the older SPB, which migrates to the daughter cell, contain an intricate network of MT plus-end interacting proteins (+TIPs; Akhmanova & Hoogenraad, 2005; Meier et al., 2024). The core of this network includes the +TIPs Kar9, Bim1, and Bik1, which couple the MT plus-end to the cargo-binding domain of type V myosin Myo2 (E. Hwang et al., 2003). The processive movement of the Kar9-Myo2 complex along actin cables toward the bud tip results in spindle alignment. To properly align the old SPB toward the bud, the cell breaks the symmetry in Kar9 localization between the aMTs of the two SPBs. Before spindle alignment, Kar9 becomes asymmetrically

biased to the aMTs of the old SPB, with reduced presence on the aMTs emanating from the new SPB (Meziane et al., 2021).

In summary, MAPs play a critical role in finely tuning the organization of MTs into specialized arrays. By differentially regulating MTs based on their spatial location and functional requirements, MAPs ensure that each array—whether involved in kinetochore attachment, spindle stabilization, or spindle positioning—is equipped with the appropriate proteins to perform its specific role. This targeted organization enables the cell to orchestrate complex mitotic processes effectively, ultimately contributing to the fidelity of chromosome segregation and the proper dynamics of the mitotic spindle during cell division.

1.4. Overview of the tubulin superfamily of proteins.

Tubulins, members of a highly conserved superfamily of proteins, are essential components of the eukaryotic cytoskeleton, where they nucleate and assemble into MTs. The tubulin superfamily comprises six families, with the most abundant being α-, β-, and γ-tubulins, which are ubiquitously expressed across eukaryotes (McKean et al., 2001). Each tubulin family includes multiple isotypes that vary not only between different organisms but also within a single organism (Janke, 2014). This review focuses on the α-, β-, and γ-tubulin families, as the remaining families—δ-, ε-, and ζ-tubulins—are significantly less abundant, often absent in many eukaryotes, and beyond the scope of this discussion.

All tubulins possess a globular domain essential for their incorporation into the MT lattice, as well as an intrinsically disordered, solvent-accessible CT domain (Nogales et al., 1998; Aldaz et al., 2005). The globular domain is highly conserved across eukaryotes, likely due to its critical role in forming the MT structure. This conservation is further highlighted by the prokaryotic tubulin homolog FtsZ, which shares a high degree of structural similarity despite sequence differences (Erickson, 1995). All tubulin globular domains feature a GTP-binding pocket in the N-terminal region. While α-, β-, and γ-tubulin each bind GTP, only β-tubulin hydrolyzes GTP to GDP at the E-site—a process linked to MT depolymerization, as GTP-bound dimers form a stabilizing cap at the MT plus-end (Aldaz et al., 2005; Gudimchuk & McIntosh, 2021; Nogales et al., 1998). In contrast, the GTP bound to α-tubulin is non-exchangeable, and the function of the GTP-binding sites in α-

tubulin has been linked to a structural role (Menéndez et al., 1998), while the γ-tubulin site remains not fully understood (Kristensson, 2021).

Conversely, the disordered CT domain is highly divergent in both sequence and length among organisms and even within tubulin families, with some organisms lacking a CT region altogether (Vogel & Snyder, 2000). Despite this variation, a common feature of all tubulin CTs is the enrichment of negatively charged residues, particularly glutamates (Roll-Mecak, 2015). The α- and β-CTs create a strongly negatively charged MT surface that regulates the binding of MAPS, which commonly contain positively charged MT-binding domains. The physicochemical differences between the α- and β-tubulin isotypes incorporated into the lattice, along with post-translational modifications within their CTs, contribute to a complex "tubulin code" that expands the functional repertoire of MTs in cells (Janke, 2014). These post-translational modifications play important roles in MT stability and interactions with MAPs. In contrast, much less is known about the biological function of the γCT, which will be explored in detail in the next section of this review.

1.5. The non-canonical, post-nucleation functions of γ-tubulin.

Decades of research in the Vogel lab have demonstrated that γ-tubulin not only nucleates MTs but also plays additional non-canonical, post-nucleation roles in forming ipMTs pairs (Shulist et al., 2017; Sim et al., 2024; Vogel et al., 2001; Vogel & Snyder, 2000). Like other tubulins, γ-tubulin contains a well-structured globular domain and an intrinsically disordered CT region (Aldaz et al., 2005). The γCT is essential for γ-tubulin function, as truncation of the entire CT region is lethal (Vogel & Snyder, 2000). Our investigations have identified a residue within the γCT—Tyrosine 445 (Y445)—that is evolutionarily conserved and phosphorylated *in vivo* (Vogel et al., 2001; Keck et al., 2011). This residue is highly conserved across fungi and metazoan γ-tubulins and is predicted to be accessible after MT nucleation (Aldaz et al., 2005; Kollman et al., 2015). Furthermore, mutating Y445 to a phospho-mimetic aspartic acid residue (Y445D) allows for WT expression of γ-tubulin (Vogel et al., 2001) and purification of stable γTuRCs (unpublished).

However, cells carrying the γ-tubulin Y445D mutation exhibit mitotic phenotypes. For instance, a double mutant of Y445D and mad1Δ (an essential component of the SAC) is lethal (Shulist et al., 2017; Vogel et al., 2001). The SAC monitors the attachment of MTs to kinetochores

and prevents the separation of sister chromatids until proper attachment is achieved. The lethality of the Y445D, mad1Δ double mutant indicates that Y445D cells require SAC activity for survival, suggesting these cells have a defect in spindle assembly. Since budding yeast γ-tubulin is known to remain stably associated with the MT minus-end throughout mitosis, this defect could potentially arise from perturbations of spindle stabilizing proteins. This is further supported by the finding that the Y445D mutation also inhibits the breakdown of the anaphase spindle (Vogel et al., 2001), indicating a specific defect in the formation of ipMTs. Indeed, subsequent genetic screens confirmed that Y445D cells are sensitive to the loss of several proteins involved in forming the ipMTs, or regulators of those proteins (Shulist et al., 2017). Notably, a synthetic lethal interaction was observed with Ase1, a highly conserved MT-bundling protein that is a core component of the yeast spindle midzone.

1.5.1. The role of γ-tubulin in the formation of the interpolar-microtubules that stabilize the midzone.

Multiple conserved eukaryotic proteins coordinate to build and maintain the spindle midzone. Ase1, the homolog of PRC1, is a non-motor MAP that can crosslink antiparallel MTs, defining the overlapping regions of ipMTs and acting as a scaffold to recruit other midzone proteins (She et al., 2019). However, although Ase1 is essential for the survival of Y445D cells, its localization is not disrupted by the Y445D mutation (Sim et al., 2024). This suggested the Y445D mutation might disrupt the function of the yeast motor protein Cin8, which has been shown to be directly recruited to the midzone by Ase1 (Khmelinskii et al., 2009) and also exhibits synthetic lethality when deleted in combination with Ase1 (Δcin8/Δase1; Shulist et al., 2017).

Cin8, a kinesin-5 family member in yeast, forms bipolar homotetrameric complexes with two MT motor domains positioned at each end of a central stalk (Hildebrandt et al., 2006; Kashlna et al., 1996; Scholey et al., 2014). The polarized structure of Cin8 allows it to bind either individual MTs, where it walks towards the minus end, or two adjacent MTs, which induces a directional switch to plus-end motility (Roostalu et al., 2011; Shapira et al., 2017). Its structure and bidirectional motility allow Cin8 molecules to both crosslink and slide MTs, which are both essential for spindle assembly and elongation (Leary et al., 2019). After spindle pole duplication

but before separation, Cin8 is the primary crosslinker of the precursor ipMTs, generating short overlaps that intersect at high angles. These crosslinks are critical for driving the eventual separation of spindle poles and the formation of the bipolar spindle (Leary et al., 2019). Following spindle pole separation, the overlapping regions of the precursor ipMTs—defined by Cin8 crosslinking—are lengthened and further stabilized by additional recruitment of both Cin8 and Ase1 (Avunie-Masala et al., 2011; Khmelinskii et al., 2009; Leary et al., 2019). At this stage, the antiparallel geometry of the MTs permits Cin8's sliding activity, which stabilizes—and later elongates—the spindle (Leary et al., 2019).

If the Y445D mutation disrupts Cin8 crosslinking, it would likely interfere with spindle pole separation. However, Y445D does not significantly delay bipolar spindle formation relative to the start of the cell cycle, nor does it reduce the maximum velocity of pole separation, suggesting that Cin8 crosslinking remains largely intact (Sim et al., 2024). Instead, the Y445D mutation produces phenotypes indicative of a Cin8 localization defect. In Y445D cells, the amount of Cin8 at the spindle midzone is significantly reduced, and its concentration is increased and biased towards the older SPB. This mislocalization correlates with reduced stability of nascent bipolar spindles in Y445D cells, which exhibit significant fluctuations in pole-to-pole length compared to WT spindles, frequently leading to partial or total spindle collapse (Sim et al., 2024). Moreover, our lab's recent structural analysis of the nascent bipolar spindle in Sim et al. (2024) using fluorophore-tagged α-tubulin (Tub1-Venus) and lattice structured illumination microscopy (SIM) revealed that the Y445D mutation is associated with reduced Tub1-Venus signal at the midzone, indicating defects in ipMT formation. Collectively, these observations suggest that the Y445D mutation compromises both Cin8 function and ipMT assembly in Y445D cells.

Interestingly, early recruitment of Ase1 to the ipMTs improves the instability of nascent bipolar spindles in Y445D cells (Sim et al., 2024). In WT cells, dephosphorylation of Ase1 drives its recruitment to the spindle, where it aids in stabilizing the ipMTs. Although inhibiting the phosphorylation of Ase1 (via an Ase1-7A mutant) in Y445D cells does not rescue the Cin8 localization defect, it increases nascent bipolar spindle stability relative to Y445D cells without Ase1-7A. This improvement is likely due to the early recruitment of Ase1 to the overlaps of precursor ipMTs, where it can crosslink MTs and support early spindle assembly, compensating

for the lack of Cin8 at the midzone. However, Ase1-7A is insufficient to support the formation of a stable midzone, likely due to the absence of Cin8 sliding forces necessary for supporting chromosome attachments. How the γCT—located at the MT minus-end—influences Cin8 localization across spindle MTs and leads to these defects remains unclear.

1.5.2. A phospho-mimetic Y445D mutation drives conformational expansion of the γCT.

While the mechanism driving these phenotypes in Y445D cells is not fully understood, there are clues about how the γCT may influence such events. Previous studies in our lab using nuclear magnetic resonance (NMR) and Monte Carlo simulations investigated how phosphorylation might affect the disordered structure of the γCT (Harris et al., 2018; Payliss et al., 2019). Although the γCT is unstructured, it predominantly adopts a collapsed state. The Y445D mutation allows the γCT to adopt unique extended conformations not seen in WT controls. Additionally, environmental pH was found to influence the likelihood of the Y445D γCT adopting the extended conformation, likely due to deprotonation of the abundant acidic residues increasing electrostatic repulsion. This suggests that both phosphorylation and specific environmental conditions *in vivo* could control the propensity for γCT extension.

Modeling the extended conformations within the entire γTuRC suggests that triggering these conformations could increase the accessibility of the γCT to binding partners after MT nucleation. Therefore, I hypothesized that the γCT interacts with proteins involved in spindle assembly and that regulation of Y445 phosphorylation influences these interactions. The position of γ-tubulin at the MT minus-end situates it ideally to serve as a point of control influencing the

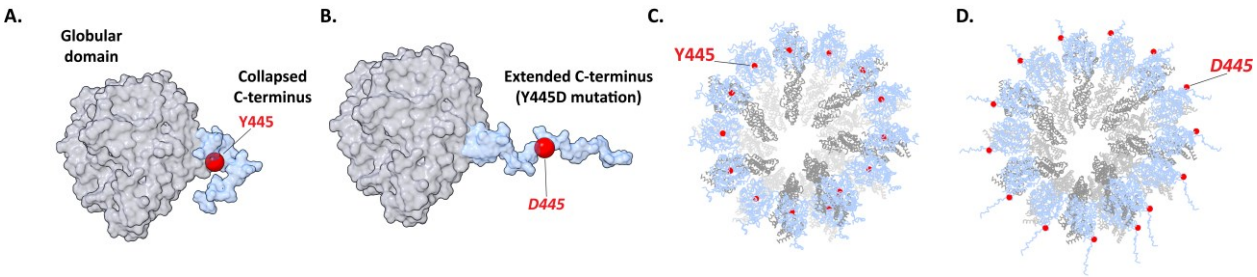

Figure 1.2. Collapsed and expanded conformations of the γ-tubulin carboxyl terminus. Representative samples of the collapsed (A and C) and expanded (B and D) γCT, as observed in Monte Carlo simulations and NMR (Harris et al. 2018), are shown both for γ-tubulin alone and within the full γTuRC (structure of the γTuRC is taken from pdb 5FLZ).

interaction of MAPs, such as Cin8, with spindle MTs. Through cell cycle-regulated phosphorylation of Y445, the γCT could function as a switch, either promoting or inhibiting MAP interactions with MTs.

This modulation could occur through direct or indirect mechanisms likely requiring extension of the γCT. For instance, phosphorylation at Y445 could promote a direct interaction between the γCT and Cin8, either recruiting Cin8 to MTs or preventing its release from the minus-end. Alternatively, phosphorylation at Y445 could regulate the interaction of Cin8 with regulatory proteins, such as Cdc28 (the budding yeast Cdk1). Indeed, Cdc28 phosphorylates Cin8 at three residues, thereby modulating Cin8's association with MTs by decreasing its affinity. Interestingly, inhibiting Cin8 phosphorylation at these residues (in the Cin8-3A mutant) exacerbates the sequestration of Cin8 to the old SPB in Y445D cells (Sim et al., 2024), supporting the possibility that Y445D disrupts the phosphoregulation of Cin8.

1.6. Searching for γ-tubulin interacting proteins: what has been done so far.

Understanding the proteins that interact with γ-tubulin is critical for elucidating the molecular mechanisms through which γ-tubulin regulates ipMT formation and influences Cin8 function. Over the years, various biochemical, genetic, and proteomic approaches have been employed to identify γ-tubulin interactors, each contributing unique insights into the composition and functional dynamics of γ-tubulin-containing complexes. However, identifying interactors beyond the well-characterized components of MTOCs has proven particularly challenging, possibly due to transient, weak, or context-specific nature of γ-tubulin interactions.

Biochemical methods such as co-immunoprecipitation and other affinity purification technologies have been fundamental in identifying physical interactions involving stable protein complexes (Rao et al., 2014). Co-immunoprecipitation relies on antibodies specific to a protein (or an epitope tag) to precipitate the protein and its associated interactors from cell lysates, followed by identification using western blotting or mass spectrometry (MS). These techniques have successfully revealed the core components of the budding yeast γTuRC, including γ-tubulin, Spc97, Spc98, and the receptor proteins Spc72 and Spc110. Other than these, there are another 40 reported physical interactors for budding yeast γ-tubulin reported on the BioGRID database.

However, applying more stringent criteria—such as requiring interactors to be supported by at least three experimental evidences or published studies—narrows the list to one well-characterized interaction with Stu2 (Greenlee et al., 2022; Gunzelmann et al., 2018). The lack of well-characterized interactions highlights how biochemical approaches have struggled to capture γ-tubulin interacting proteins beyond other MTOC components.

This relatively limited pool of consistently identified interactors underscores the limitations of traditional biochemical methods in capturing the full range of γ-tubulin's interactome. Thus, I hypothesize that additional γ-tubulin interactions are potentially mediated through the γCT, which is highly disordered and predicted to be accessible to binding partners after a MT has formed (Aldaz et al., 2005; Kollman et al., 2015). In contrast, the globular domain of γ-tubulin is more likely to be stably associated with other γTuRC components and tubulin heterodimers, limiting its involvement in interactions outside the ring complex. As γ-tubulin remains anchored to the MT minus-end throughout mitosis, mutations such as γ-tubulin Y445D, which disrupts Cin8 interactions across the length of MTs, may influence interactions mediated through the γCT.

Disordered regions, such as the γCT, possess conformational plasticity that enables them to engage in a broad spectrum of potential interactions compared to more structured proteins (Acuner Ozbabacan et al., 2011; Lee et al., 2014). This conformational flexibility is why proteins acting as signaling hubs are often intrinsically disordered. However, the transient and weak nature of these numerous interactions makes them difficult to detect using standard biochemical methods. To overcome this challenge, advanced techniques like proximity-labeling approaches—such as BioID—are essential for capturing a more comprehensive spectrum of γ-tubulin-associated proteins *in vivo* (Branon et al., 2018; Roux et al., 2012, 2018).

1.7. Protein interaction screens using the proximity-labeling method BioID.

The difficulty in detecting transient or weak protein interactions using traditional screens led to the development of methods designed to capture these fleeting associations. One such method is BioID, a proximity-labeling technique that uses a mutant form of the *Escherichia coli* (*E. coli*) biotin ligase, BirA (BirA-R118G, also called BirA*) (Roux et al., 2012). In *E. coli*, WT BirA

catalyzes a reaction between biotin and ATP to produce biotinyl-5'-AMP (bioAMP), holding it in its active site. This bioAMP is then transferred to a lysine residue on a target protein at a specific recognition motif. However, the BirA-R118G mutation disrupts this motif recognition and lowers biotin affinity, causing BirA* to freely convert biotin to bioAMP and promiscuously biotinylate nearby proteins. BirA* activates biotin and covalently tags proteins within a ~10–15 nm radius, even if the interactions are transient or low-affinity (Roux et al., 2012, 2018). These biotinylated proteins can be efficiently isolated via the high-affinity biotin-streptavidin interaction (Kd = 10^{-14} M; Green, 1963) and identified by MS, offering a more comprehensive view of protein interactions in their native cellular context. In addition to BirA*, several other BirA variants have been produced through directed evolution to create biotin ligases with altered properties, such as increased enzymatic activity (J. Hwang & Espenshade, 2016; Branon et al., 2018). These engineered ligases enhance the efficiency of proximity-labeling techniques like BioID, enabling faster and more extensive biotinylation of proximal proteins.

1.8. Motivation and aims.

Given that γ-tubulin remains associated with the MT minus-end throughout mitosis, I hypothesized that the γCT interacts with proteins involved in spindle assembly and that regulation of Y445 phosphorylation modulates these interactions. However, few γ-tubulin interactions have been identified beyond components of the MTOCs, posing a challenge for characterizing the γCT mechanism that influences Cin8 function. Additionally, I propose that additional γ-tubulin interactions are likely mediated through the γCT, as the globular domain is predominantly involved in templating MT nucleation. To address these gaps, I will adapt and optimize a yeast TurboID method to detect γ-tubulin interactors and examine the impact of the Y445D mutation on these interactions.

CHAPTER 2 – METHODOLOGY

2.1. Yeast strain construction and strains.

All yeast strains were constructed using the lithium acetate-based transformation protocol (Daniel Gietz & Woods, 2002)in the haploid strain BY4741 (mat A). PCR amplified cassettes were

used to integrate tags and transformants were selected using auxotrophic markers. Sequential transformations were performed to integrate either ADH1-OsTIR1-URA3 or ADH1-OsTIR1-F74G-URA3 into the HIS locus, C-terminally tag Bpl1 with AID-6HA-HYGR, and C-terminally tag bait proteins with TurboID. For the mNeonGreen-TurboID noise control, in lieu of a bait protein, Gibson assembly was used to create an mNeonGreen-TurboID cassette, which was subsequently integrated into the deleted URA locus.

- SPC97-TurboID-3xMyc-KANMX6; BPL1-AID-6HA-HYGR; HIS3::ADH1-OsTIR1-URA3; MATa; his3Δ1; leu2Δ0; ura3Δ0; met15Δ0
- CIN8-TurboID-3xMyc-KANMX6; BPL1-AID-6HA-HYGR; HIS3::ADH1-OsTIR1-URA3; MATa; his3Δ1; leu2Δ0; ura3Δ0; met15Δ0
- ADH1-mNG-Flag-TurboID-S.p.HIS5; BPL1-AID-6HA-HYGR; HIS3::ADH1-OsTIR1-URA3; MATa; his3Δ1; leu2Δ0; ura3Δ0; met15Δ0
- BPL1-6HA-AID-HYGR; HIS3::ADH1-OsTIR1-URA3; MATa; his3Δ1; leu2Δ0; ura3Δ0; met15Δ0

After exchanging the original AID technology with the newer AID2, the genotypes used were:

- SPC97-TurboID-3xMyc-KANMX6; BPL1-AID-6HA-HYGR; HIS3::ADH1-OsTIR1(F74G)-URA3; MATa; his3Δ1; leu2Δ0; ura3Δ0; met15Δ0
- CIN8-TurboID-3xMyc-KANMX6; BPL1-AID-6HA-HYGR; HIS3::ADH1-OsTIR1(F74G)-URA3; MATa; his3Δ1; leu2Δ0; ura3Δ0; met15Δ0
- ADH1-mNG-Flag-TurboID-S.p.HIS5; BPL1-AID-6HA-HYGR; HIS3::ADH1-OsTIR1(F74G)-URA3; MATa; his3Δ1; leu2Δ0; ura3Δ0; met15Δ0
- BPL1-6HA-AID-HYGR; HIS3::ADH1-OsTIR1(F74G)-URA3; MATa; his3Δ1; leu2Δ0; ura3Δ0; met15Δ0

2.2. Protein extraction and western blot analysis.

For western blot analysis, proteins were extracted from yeast cells as previously described in Kushnirov (2000) and separated on 4-20% Tris/Glycine precast polyacrylamide gels using SDS-PAGE. Proteins were transferred to PVDF membranes and incubated for 1 hour with the following: biotinylated proteins were detected using fluorescent Streptavidin 800CW IRDye (1:10,000 in 5%

w/v BSA/PBS); Myc-tagged bait proteins (Spc97 and Cin8) were detected using mouse anti-Myc primary antibody (1:1,000 in 5% w/v powdered milk) followed by anti-mouse 680 IRDye secondary antibody (1:10,000 in 5% w/v powdered milk); Bpl1-HA protein was detected similar to the Myc-tagged proteins, but using mouse anti-HA. Blots were washed and imaged on a LI-COR Odyssey Infrared scanner, then band intensities were quantified using ImageJ.

2.3. Biotinylation and preparation of yeast lysates by cryogenic ball milling.

Yeast cells were cryo-lysed to preserve transient interactions and protein complexes in native conditions. Yeast strains were each grown at 25^{o}C with shaking overnight in 400 mL of Synthetic Complete media. The following morning, mid-log phase cultures were back-diluted to OD600 0.1 into a final volume of 2L of SC media supplemented with 100 nM of biotin and 1 mM of auxin (for AID) or 5 µM of 5-Ph-IAA. Cells were grown at 30^{o}C with shaking for approximately 4 hours and collected in mid-logarithmic phase (OD600 ~0.5). As the Y445D mutation has been known to increase cell size, cells were counted for WT strains at an OD600 of ~0.5, and Y445D cells were counted and harvested at an equivalent number. Cell pellets were rapidly frozen by immersing into liquid nitrogen, and then mechanically ground in a frozen state using a planetary ball mill. Frozen cell grindate was stored at -80^{o}C until subsequent processing.

2.4. Affinity capture of biotinylated proteins and LC-MS/MS sample preparation.

Protease-resistant streptavidin-conjugated Sepharose beads were generated by chemical modification of lysine and arginine residues (Rafiee et al., 2020). For each strain, 1.5g of frozen yeast grindate was slightly thawed on ice and vortex-resuspended into 13.5 mL of extraction buffer [20 mM HEPES pH 7.4, 110 mM KOAc, 0.5% Triton X-100, 0.1% Tween 20, 1:100 Solution P, 1:5000 Antifoam B, 100 mM NaCl]. Resuspended grindate was further homogenized on ice for 30 seconds using a polytron and cleared by centrifugation at 4^{o}C for 10 minutes at 4,000 g. For affinity purifications, 4 mL of cleared lysate was incubated with 50 µL of washed protease-resistant streptavidin beads in triplicate for 1 hour at 4^{o}C with rotation. Beads were collected in fresh 1.5 mL LoBind Eppendorf tubes, washed four times with 1 mL of extraction buffer and then five times in wash buffer [0.1 M ammonium acetate pH 7.5] for 5-minute intervals with rotation

at 4°C. Beads were resuspended in 100 mM ammonium bicarbonate at pH 8.0. The samples were reduced with 5 mM of dithiothreitol for 30 minutes at 37°C with 350 rpm shaking, then acetylated in the dark with 16 mM of iodoacetamide at room temperature for 30 minutes. Finally, the beads were incubated overnight with 1 µg of sequencing-grade Trypsin at 37°C and 350 rpm shaking. The following morning, samples were spiked with an additional 0.5 µg of Trypsin and incubated for a further 2 hours at the same conditions. Beads were gently centrifuged for 1 minute at 500 g at room temperature and the supernatant was transferred to a fresh 1.5 mL LoBind tube. The beads were rinsed twice with 100 µL of mass spectrometry (MS) grade water and the washes were pooled with the collected supernatant. The digestion was quenched by addition of 50% stock formic acid to a final concentration of 5%. To remove any remaining streptavidin, the samples were spun for 10 minutes at max speed and the supernatant was transferred to a fresh tube three times. The peptides were vacuum dried by centrifuging in a SpeedVac at room temperature and stored at -20°C until further analysis.

2.5. LC-MS/MS settings and analysis.

The supernatants were acidified with trifluoroacetic acid and cleaned from residual detergents and reagents with MCX cartridges (Waters Oasis MCX 96-well Elution Plate) following the manufacturer's instructions. After elution in 10% ammonium hydroxide/90% methanol (v/v), samples were dried with a Speed-vac. Samples were resuspended in 15 µL of 5% formic acid for the LC-MS/MS analysis. For each series of samples, a LC-MS/MS analysis using a short gradient has been performed on at least one diluted sample (1:20) to evaluate the concentration of peptides and decide on the highest volume to be injected for the full gradient analysis for reaching the maximum sensitivity without saturating the LC-MS/MS system. Samples were loaded into a 75 µm internal diameter × 150 mm Self-Pack C18 column installed on the Easy-nLC II or the Easy-nLC 1000 system (Proxeon Biosystems). The buffers used for chromatography were 0.2% formic acid (solvent A) and 100% acetonitrile/0.2% formic acid (solvent B). Peptides were eluted with a three-slope gradient at a flowrate of 250 nL/min. Solvent B first increased from 3 to 15% in 45 min, then from 15 to 34% in 64 min and finally from 34 to 60% B in 8 min. The HPLC system was coupled to a Orbitrap Fusion mass spectrometer (Thermo Scientific) through a Nanospray Flex

Ion Source. Nanospray and S-lens voltages were set to 1.3-1.7 kV and 50-60 V, respectively. The capillary temperature was set to 250°C. On the Orbitrap Fusion, full scan MS survey spectra (m/z 360-1560) in profile mode were acquired in the Orbitrap with a resolution of 120 000 and the AGC target at $3x10^5$. The 25 most intense peptide ions were fragmented in the HCD collision chamber at a normalized collision energy of 29 and MS/MS spectra were analyzed in the linear trap with the AGC target at $2x10^4$ and the dynamic exclusion set to 8 seconds.

2.6. LC-MS/MS raw data processing and analysis.

Protein database searching of raw data was performed using MaxQuant v.2.4.3.0 against the UniProt *S. cerevisiae* ATCC 204508 / S288c database (August 2023 version, 6060 entries). Oxidation of M, protein N-term acetylation, and phosphorylation of STY residues were set as variable modifications. Carbamidomethylation of C was set as a fixed modification. Trypsin/P was used as the enzyme with a maximum of 3 missed cleavages allowed. Peptide spectral match (PSM) and protein false discovery rates (FDRs) were set at a 1% threshold and estimated using a target-decoy strategy. Data analysis was performed in Perseus v2.0.9.0. Decoy and contaminant hits were filtered out, as well as proteins identified based on a modified peptide only. Prey proteins with < 3 identified total peptides were also filtered out. Protein intensities were log2-transformed and only proteins with at least two valid values in at least one experimental group were kept. The remaining missing values were imputed using a low-range random distribution. Unpaired student's t-tests were used to calculate significance values and log2 fold-changes between experimental groups. Volcano plots of prey proteins were generated using the webtool VolcaNoseR (https://huygens.science.uva.nl/VolcaNoseR/) and dot plots were generated using the ProHits-viz webtool (https://prohits-viz.org/). Protein network analysis was performed by searching high-confidence interactions of Cin8 on the STRING database using Cytoscape software. Cluster analysis was performed in Cytoscape v3.10.2 using the ClusterMaker tool and Markov cluster algorithm with default settings.

CHAPTER 3 – RESULTS

3.1. Adaptation of yeast BioID for γ-tubulin interaction studies.

To investigate the role of the γCT in ipMT assembly and Cin8 function, I adapted a yeast-optimized BioID method, designed to detect transient and weak interactions in yeast (Fenech et al., 2023). BioID has been used sparingly in yeast due to highly abundant, endogenous enzymes that are essential and natively biotinylated (Figure 2.1A). These enzymes generate a high background signal when detecting biotinylated proteins, reducing the signal-to-noise ratio and making it difficult to identify specific interactors. However, as demonstrated by Fenech et al. (2023), an auxin-inducible degron (AID) system can be used to deplete the essential protein Bpl1, the sole yeast biotin ligase, thereby preventing its substrate interactions and decreasing the background biotinylation (Figure 2.1B). Furthermore, BirA* exhibits optimal activity at a temperature of 37°C, while ideal growth conditions for yeast range from 25-30°C. Fortunately, a variant of BirA, named TurboID, was produced through directed evolution in yeast, and is both optimally active at 30°C and generates significantly higher signal compared to BirA* (Branon et al., 2018). In combination with Bpl1-AID degradation and the increased activity of the TurboID,

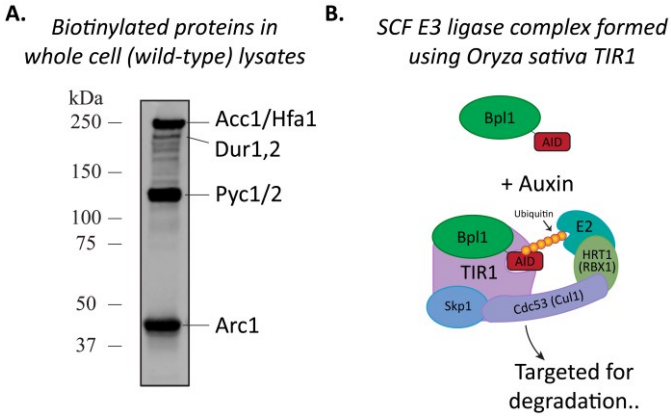

Figure 3.1. The yeast biotin ligase, Bpl1, biotinylates endogenous enzymes. A. Natively biotinylated endogenous enzymes in budding yeast are highly abundant (detected on western blot using Streptavidin IRDye), reducing the signal-to-noise during MS analysis. **B.** The yeast biotin ligase Bpl1 can be targeted for degradation by the proteasome using an AID system, decreasing the levels of native biotinylation and increasing the MS signal-to-noise.

this method increases the signal-to-noise and enhances the detection of candidate interactors in yeast.

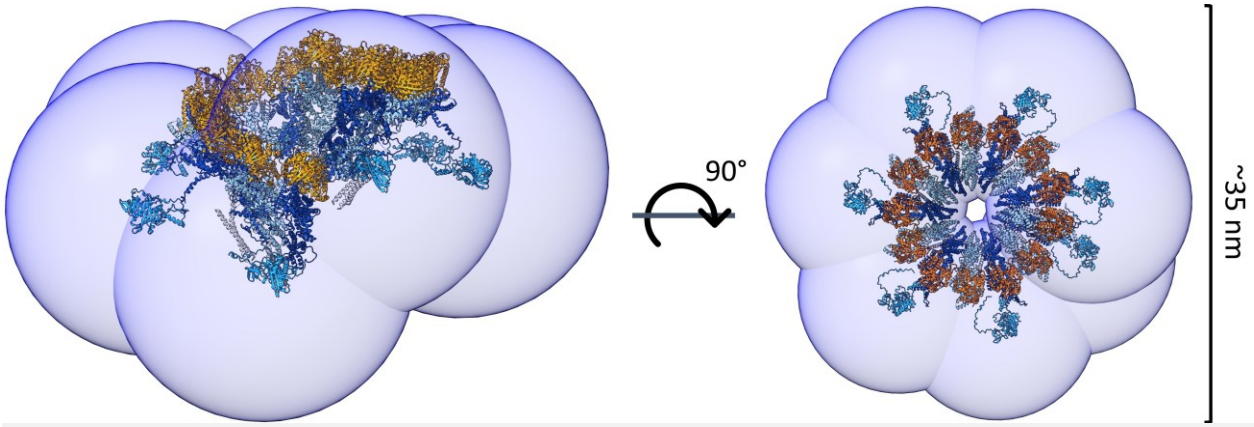

Figure 3.2. TurboID fused to Spc97 promiscuously biotinylates proteins within a 15 nm radius. AlphaFold2 was used to generate a predicted TurboID structure (colored in teal). ChimeraX was used to attach the predicted TurboID model to each Spc97 (colored in orange) within the γTuRC (structure of the γTuRC was taken from pdb 5FLZ), separated by an eight-residue Glycine-Serine linker. Transparent blue spheres, each representing a 15 nm radius from the center of each TurboID, were used to visualize the potential proximity labeling range around each TurboID. Note that flexibility in the linker may extend this radius slightly.

To implement this, I fused an auxin-inducible degron (AID) to the C-terminus of Bpl1 (Bpl1-AID-HA) and expressed *Oryza sativa* TIR1 (OsTIR1) from a chromosomal locus (Nishimura et al., 2009). I selected the γTuRC component Spc97 as the TurboID bait to detect γ-tubulin interactors (Figure 2.2), as the C-terminus of Spc97 is more tolerant of tags compared to γ-tubulin, where tagging the γCT could disrupt potential interactions. I anticipated that proteins interacting with γ-tubulin would fall within the diffusion radius of Spc97-TurboID labeling because: 1) γ-tubulin is stably associated with the Spc97 C-terminus in the γTuRC throughout mitosis; and 2) Monte Carlo simulated models suggest the maximal extension of the γCT is less than 10 nm, well within the predicted TurboID labeling radius (Branon et al., 2018; Harris et al., 2018). Using this strain, I measured Bpl1-AID-HA degradation in cells supplemented with 1 mM auxin. Western blot quantification revealed a 71.5 ± 7.4% reduction in the Bpl1 WT signal, corresponding to a marked decrease in several prominent bands, including Acc1 (Acetyl-CoA carboxylase), the most abundant natively biotinylated enzyme (Figure 2.3).

After having successfully reduced the native level of biotinylation by degrading BPL1-AID-HA, I made two key modifications to the method for my purposes. First, I adapted the approach

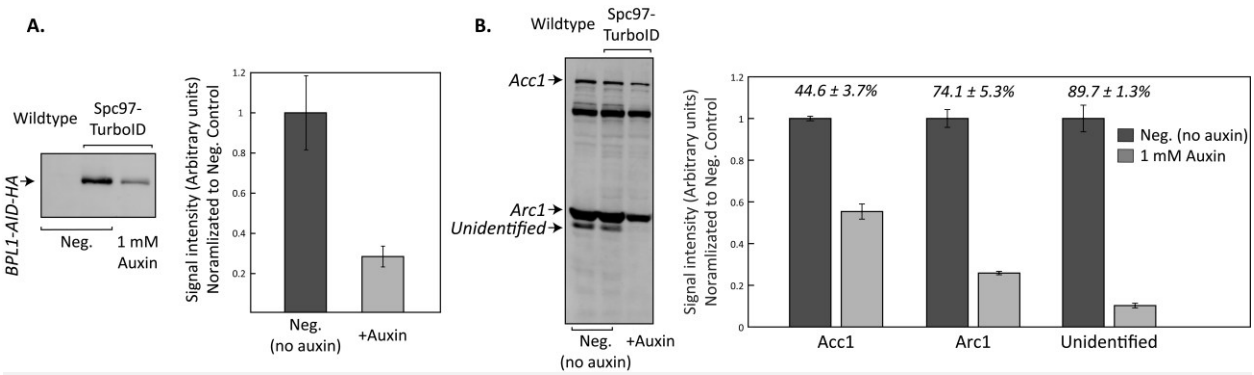

Figure 3.3. An auxin-inducible degron degrades Bpl1 and reduces native biotinylation levels. Spc97-TurboID cells were cultured in the absence and presence of 1 mM auxin, alongside a WT negative control strain (no auxin). Cell lysates were separated by SDS-PAGE in triplicate, and **(A)** BPL1-AID-HA was detected using an anti-HA antibody, while **(B)** biotinylated proteins were detected using streptavidin-conjugated IRDye. Bar plots to the right of the respective western blots present quantification of the detected signals using ImageJ.

by Rafiee et al. (2020) to chemically modify streptavidin-conjugated beads. A common issue with BioID methods is the significant background signal caused by proteolysis of streptavidin, which generates intense peptides that can saturate the MS signal, reducing sensitivity and masking peptides of interest. This method uses lysine demethylation and arginine condensation to block cleavage at these residues, which are targeted by commonly used proteases like trypsin. This approach was shown by Rafiee et al. to reduce streptavidin contamination by 100- to 1000-fold, significantly decreasing background signal and enhancing sensitivity.

Second, I implemented yeast cryo-grinding (Figure 2.4), a highly efficient and consistent lysis technique, along with mild denaturation conditions, as opposed to the harsher conditions typically used in BioID experiments. The tough cell wall of budding yeast is difficult to break with traditional methods like bead-beating, which can result in suboptimal release of nuclear proteins.

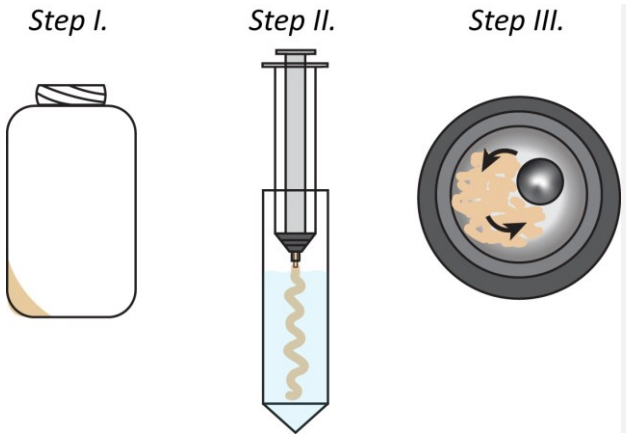

Figure 3.4. The yeast biotin ligase, Bpl1, biotinylates endogenous enzymes. Yeast cells are frozen in liquid nitrogen and lysed by cryo-grinding to produce debris which preserves transient interactions and protein complex structures. Cell culture is pelleted (Step I) and syringed directly into liquid nitrogen (-196°C) to create brittle “yeast noodles” (Step II; the increased surface area improves the lysis efficiency). The yeast noodles are then lysed using a planetary ball mill in cryo-genic conditions (Step III; top-view of grinding jar with steel ball and yeast noodles).

Cryo-grinding addresses this by submerging yeast pellets in liquid nitrogen, followed by lysing the frozen cells in a ball mill using mechanical shear and impact forces (Figure 2.4). These forces are sufficient to lyse more than 95% of cells without degrading proteins, producing fine particulate debris consisting of disrupted cell membranes, organelles, and proteins. This approach ensures the complete disruption of cellular membranes and maximal release of proteins, including nuclear proteins. Additionally, because of the strong affinity between streptavidin and biotin, BioID methods often use harsher buffer conditions to fully solubilize membranes and proteins. However, since our proteins of interest are not membrane-bound, I reasoned that milder buffer conditions, similar to those in co-immunoprecipitation experiments, would better preserve transient interactions and native protein complexes. This approach could provide a more comprehensive view of the proteins interacting with our bait and the pathways they may be involved in.

In addition to the Spc97 bait, I constructed two control strains: a background control (BgCtrl, lacking the TurboID enzyme) and a noise control (mNG-TurboID, or mNeonGreen-TurboID). The background control accounted for signals from natively biotinylated proteins and non-specific binding to the agarose beads, while the noise control, constitutively expressed from a chromosomal locus and diffuse in the cytoplasm and nucleus, helped control for false-positive interaction identifications. I also prepared a Cin8-TurboID bait strain, expecting that if the γCT

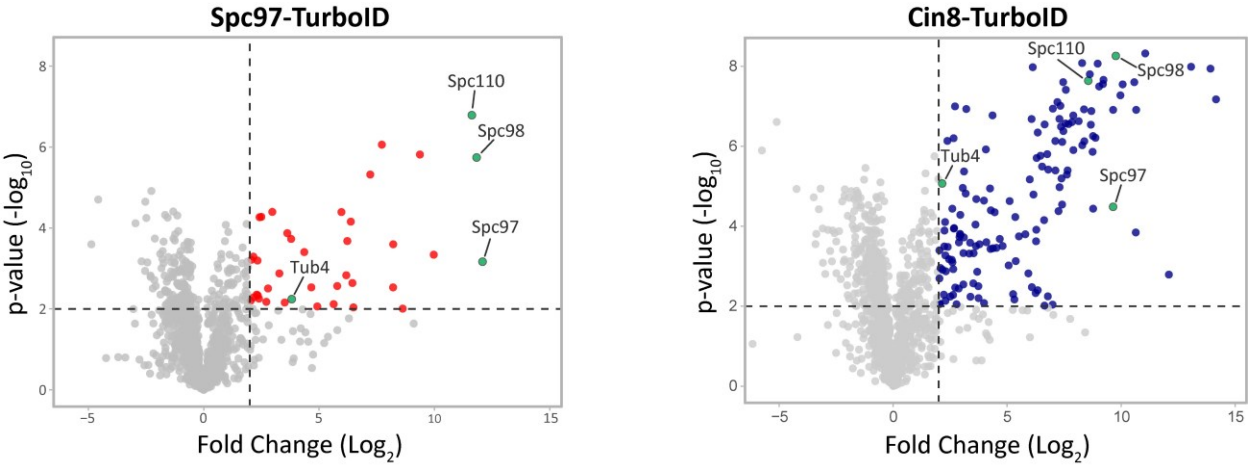

Figure 3.5. Enrichment of prey proteins detected using Spc97 and Cin8 baits against controls. These volcano plots show proteins identified in Spc97 and Cin8 TurboID screens. Proteins highlighted in the plot were significantly enriched (log2 fold-change ≥ 2.0 and p-value ≤ 0.05) compared to a background control (no TurboID enzyme). The locations of γTuRC proteins Spc97, Spc98, and γ-tubulin are also indicated in the plot.

directly associates with Cin8 to influence its localization, both Cin8 and γ-tubulin would be mutually detected in their respective screens. I performed the optimized experiment using these four strains and analyzed the enriched biotinylated proteins via MS (Figure 2.5).

After MS analysis, raw chromatograms were compared against a database of the *S. cerevisiae* proteome using MaxQuant, which generated peptide and protein identifications using a False Discovery Rate threshold of 1%. The relative amounts of identified proteins in the bait strains were compared to the background and noise controls using label-free quantification. Protein identifications were considered significant if the bait signal exceeded a $\log_2$ fold-difference of ≥ 2.0 and p-value ≤ 0.05 relative to the protein's signal in the background and noise controls in triplicate. The TurboID screens generated a list of 33 and 139 significant protein identifications for the Spc97 and Cin8 baits, respectively. Importantly, both the Spc97 and Cin8 screens identified interactions with all three γTuRC components and the nuclear SPB receptor Spc110. However, surprisingly, Cin8 was not detected in the Spc97 screen. A possible explanation is that Cin8-TurboID can label up to seven copies of Spc97 per within the γTuRC per interaction, whereas Spc97-TurboID can label only four Cin8 per interaction, resulting in a lower signal. Additionally, the lower abundance of Cin8 (median 763 ± 682 molecules/cell) compared to Spc97, Spc98, and γ-tubulin (median 1794 ± 378, 1528 ± 710, and 3148 ± 1751 molecules/cell, respectively)—as reported on the Saccharomyces Genome Database (Cherry, 1998)—may have hindered its detection by MS due to masking by higher abundance proteins (such as Acc1; refer to Section 4.1 for a discussion of this issue).

Furthermore, the Cin8-TurboID screen identified a variety of proteins, highlighting Cin8's diverse roles in spindle dynamics. Most notably, Cin8-TurboID identified several proteins involved in forming and regulating the dynamics of midzone ipMTs. These interactions included other kinesins, such as the minus-end-directed Kar3 and its light chain Vik1, as well as the plus-end-directed kinesin Kip3. In addition, Cin8-TurboID detected proteins associated with kinetochores or kMTs, including CBF1, CBF2, Stu1, Stu2, and the DASH/DAM1 complex. This aligns with Cin8's known role in mediating kMT length, where it moves toward the plus-end of kMTs during the search-and-capture phase and acts as a length-dependent kMT depolymerase (Gardner et al., 2008). In conclusion, these preliminary findings suggested that this method effectively detects

interactions along the entire length of spindle MTs and could provide valuable insights into how γ-tubulin influences Cin8's interactions with MTs, and potentially with other associated proteins.

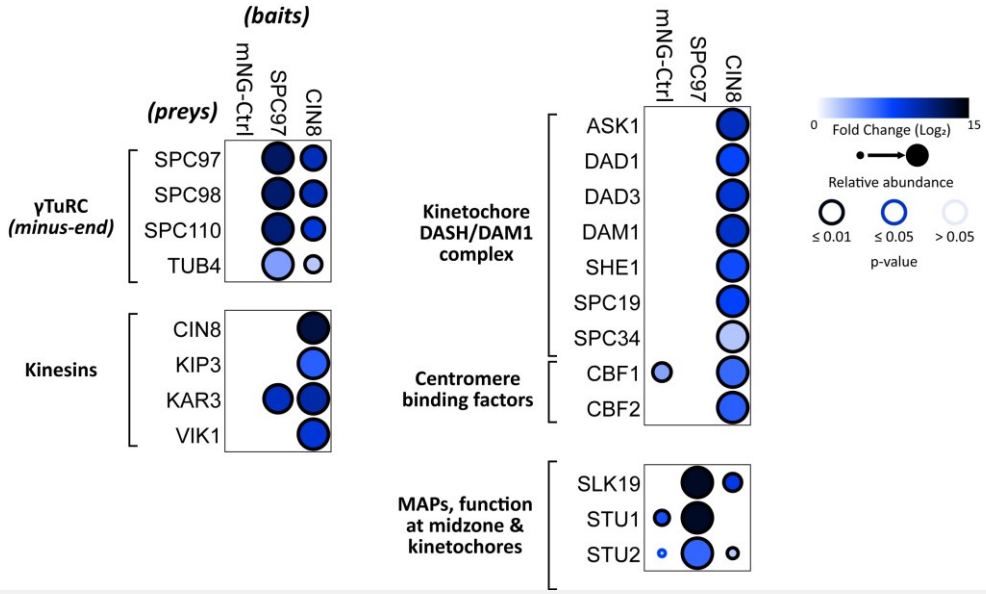

Figure 3.6. Spc97- and Cin8-TurboID screens identify proteins which function across the length of MTs. Curated proteins detected in Cin8 and Spc97 preliminary experiment. These were significantly enriched against background and noise controls in triplicate experiments using label-free quantification.

3.2. Degradation of Bpl1 by AID2 technology improves the reduction of native biotinylation.

To improve the reduction of native biotinylation, I utilized the recently developed AID2 system (Yesbolatova et al., 2020). The original AID system, introduced by Nishimura et al. in 2009, enables controlled protein degradation by tagging proteins with a degron. This degron triggers rapid degradation in the presence of the plant hormone auxin and the *Oryza sativa* F-box protein TIR1 (OsTIR1), which facilitates ubiquitination and proteasomal degradation of the target protein. However, the AID system has two major limitations: leaky degradation, where degron-tagged proteins undergo partial degradation even in the absence of auxin (particularly an issue for essential proteins, like Bpl1), and the need for high auxin concentrations (1 mM in yeast), which can cause acute short-term effects on cell lines. To address these issues, Yesbolatova et al. (2020) developed the AID2 system, which employs a mutant OsTIR1(F74G) in combination with the auxin analogue 5-Ph-IAA, which significantly increases sensitivity and eliminates leaky degradation. I replaced the WT OsTIR1 in my BioID strains with the OsTIR1(F74G) mutant and repeated the noise reduction experiments using 5 µM of 5-Ph-IAA. Western blot quantification showed a marked

improvement in the reduction of ACC1 biotinylation (Figure 2.7), with a signal decrease of 69.0 ± 3.5% in the Spc97 bait strain and 65.3 ± 2.6% in the Cin8 bait strain (relative to a control with no 5-Ph-IAA).

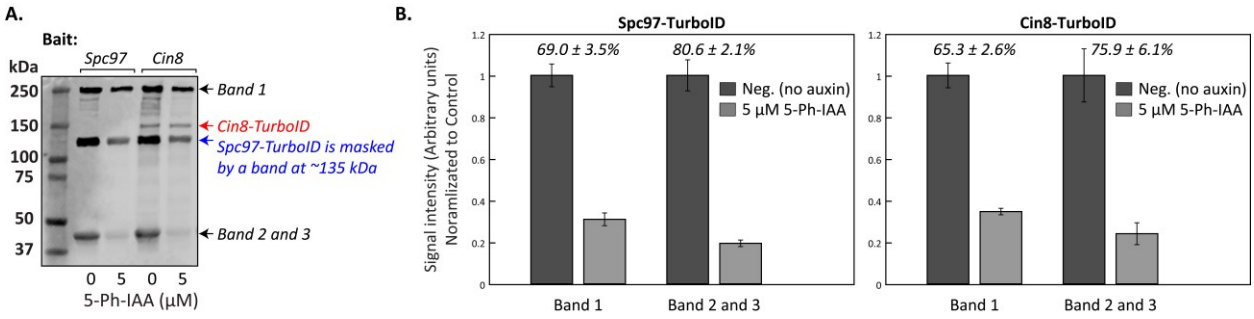

Figure 3.7. Degradation of Bpl1 using AID2 technology improves the reduction of native biotinylation. Spc97-TurboID and Cin8-TurboID cells carrying the AID2 system for targeted Bpl1-AID2-HA degradation were cultured both in the absence and presence of 5 μM 5-Ph-IAA (an auxin analogue). **(A)** Cell lysates were separated by SDS-PAGE in triplicate, and biotinylated proteins were detected using streptavidin-conjugated IRDye. **(B)** Quantification of the detected signals was performed using ImageJ, and the results are displayed in bar plots.

3.3. A general survey of the Spc97 and Cin8 interactomes as identified using yeast TurboID.

Next, I aimed to identify interacting proteins of Spc97 and Cin8 in γ-tubulin WT and Y445D backgrounds using the optimized method. I was unable to generate viable haploids carrying both Spc97-TurboID and γ-tubulin Y445D, likely indicating a synthetic lethal relationship. The γ-tubulin Y445D mutation has been shown to be synthetically lethal with various mutations and gene deletions, so this outcome was not unexpected. I hypothesize that attaching a TurboID protein to all units of Spc97 in the ring introduces additional steric hindrance, potentially disrupting interactions within the ring or with proteins that potentially associate with the γTuRC. This disruption may reduce cellular fitness. When combined with the fitness reduction caused by the Y445D mutation, the cumulative effect could result in a synthetic lethal interaction which prevents the generation of viable haploids. A potential workaround could involve expressing an additional Spc97 gene fused to TurboID, which might dilute the number of TurboID-tagged Spc97 molecules within a single γTuRC. However, I proceeded with the Cin8-TurboID; γ-tubulin Y445D strain to focus on investigating how the Y445D mutation affects the interactome of Cin8, as this approach would still yield valuable insights into how Y445D influences Cin8 function. I performed two additional MS experiments: the first analyzed the same strains as before—Spc97-TurboID,

Cin8-TurboID, mNG-TurboID, and BgCtrl (Figure 2.8 and 2.10-11)—while the second focused on Cin8-TurboID, comparing strains with γ-tubulin WT and Y445D, alongside the BgCtrl (Figure 2.9 and 2.13). This resulted in a total of 57 significant protein identifications for Spc97-TurboID, with 9 proteins detected in both experiments, and 426 for Cin8-TurboID, with 82 overlapping across all three experiments.

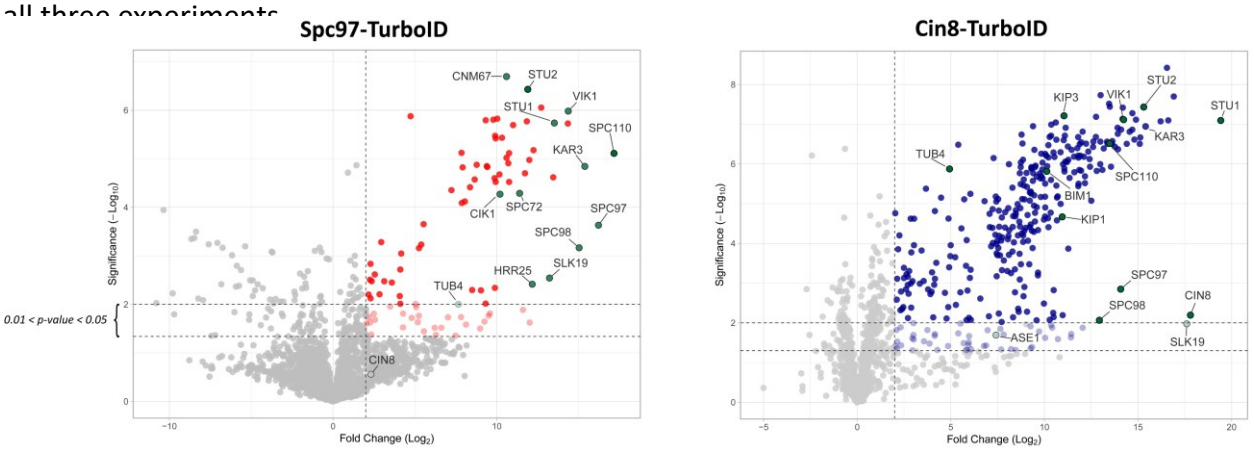

Figure 3.8. Spc97 and Cin8 interact with proteins involved in spindle structure and dynamics. These volcano plots display proteins identified in Spc97 and Cin8 TurboID screens in strains using the AID2 system. Proteins highlighted in the plots were significantly enriched (log2 fold-change ≥ 2.0 and p-value ≤ 0.05) compared to a background control (no TurboID enzyme, x-axis) and noise control (mNeonGreen-TurboID, not displayed). The locations of the γTuRC proteins—Spc97, Spc98, and γ-tubulin—as well as other curated proteins involved in spindle assembly and stability, are also marked in the plots.

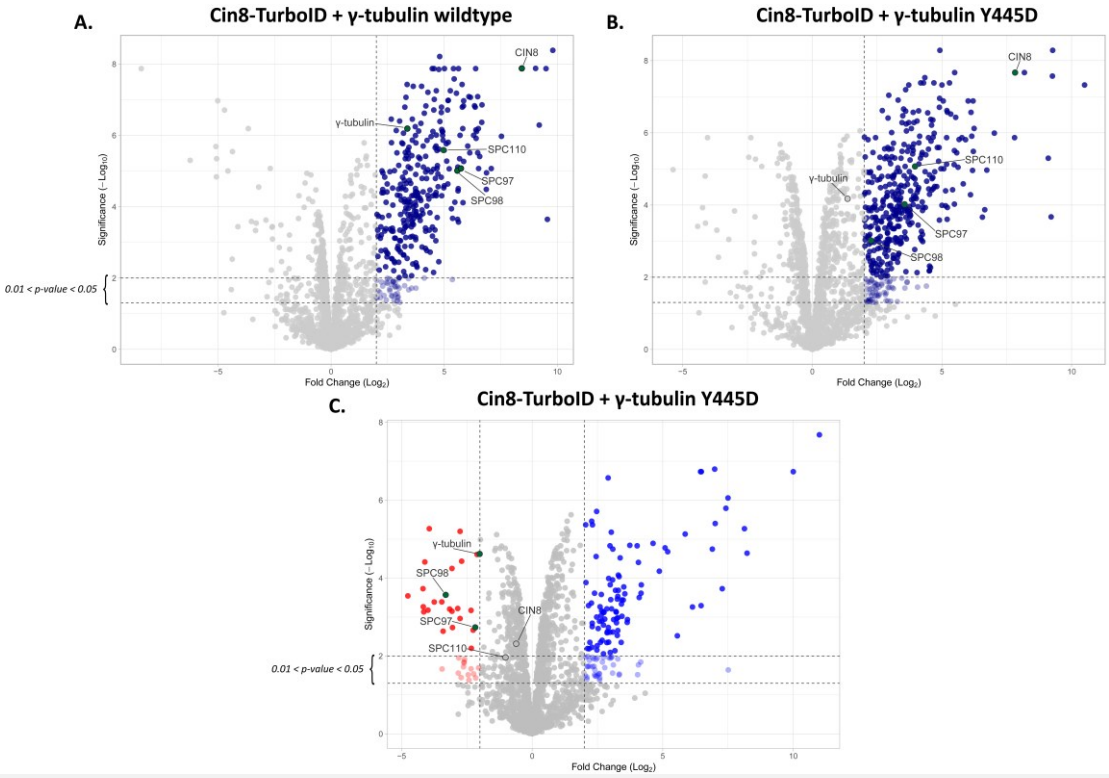

Figure 3.9. Cin8-TurboID detects less γTuRC signal in the presence of a γ-tubulin Y445D mutation. These volcano plots show proteins identified in Cin8-TurboID screens for strains with γ-tubulin WT **(A)** and the Y445D mutation **(B)**. The signal of prey proteins in the Y445D background is compared to the WT γ-tubulin on a log2 fold-change scale in **(C)**. Proteins highlighted in the plots were significantly enriched (log2 difference of ≥ 2.0 and p-value ≤ 0.05) compared to a background control (no TurboID enzyme) and noise control (mNeonGreen-TurboID, not displayed). The locations of γTuRC proteins—Spc97, Spc98, and γ-tubulin—and Cin8 are also indicated in the plots.

Spc97-TurboID identifies spindle proteins, MAPs, and potential novel interactions.

Among the hits for Spc97 (Figure 2.10), all three γTuRC components and the nuclear SPB receptor Spc110 were consistently detected. However, unlike the previous screen, several components of the SPB outer plaque were also detected, including Cnm67, Nud1, and Spc72, the outer plaque γTuRC receptor protein. Mlp2, a component of the nuclear envelope, which lays adjacent and connects to the SPB, was also detected. Additionally, several proteins with spindle function that localize to the midzone were identified, with only Stu2 having been previously shown to interact with γ-tubulin. However, like before, Cin8 signal did not exceed the significance thresholds. The other proteins—Slk19, Stu1, Kar3, Cik1, Vik1, and Fin1—have not been previously shown to interact with any components of the γTuRC. Of these proteins, several contribute to

stability of the spindle during metaphase, most notably, Kar3, a minus-end-directed Kinesin-14 motor protein, which crosslinks ipMTs and facilitates their alignment along the spindle axis, ensuring proper spindle assembly. Additionally, the light chains of Kar3 were detected, Cik1 and Vik1, which form dimers with Kar3 and control its spindle localization and function.

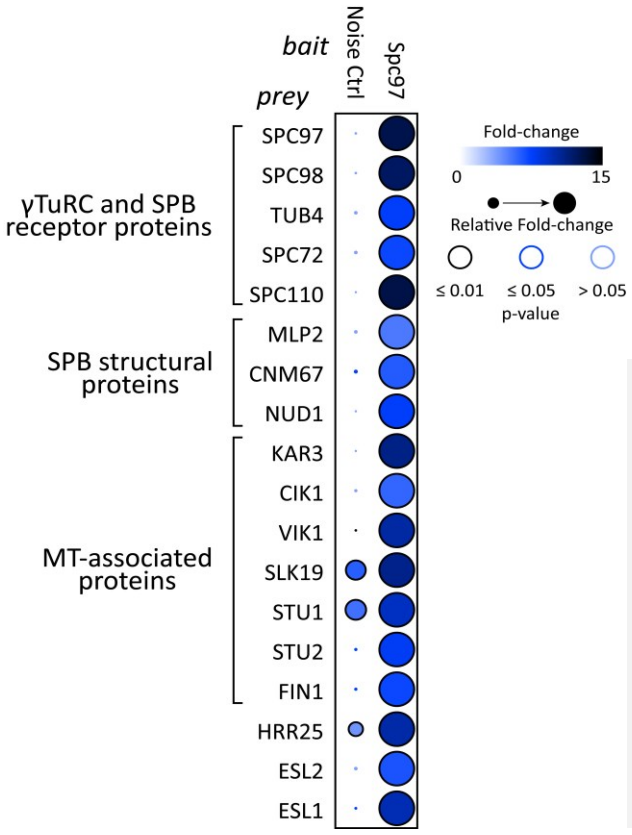

Figure 3.10. Curated proteins identified using a Spc97 bait with yeast-optimized TurboID. Select interactors identified in the Spc97-TurboID screen are shown in a dot plot. The class of each protein is indicated to the left of the identified (or prey) protein names. The relative enrichment of protein signals, comparing the Spc97 bait and a noise control (mNeonGreen-TurboID) against a background control (no TurboID enzyme), is displayed on a log2 scale. The size of the circle in each row reflects the relative abundance of the protein within the strain corresponding to each column.

Of note, an interaction with the kinase HRR25 (yeast Casein Kinase I) was detected, corroborating a previous report of an interaction with γ-tubulin (Peng et al., 2015). HRR25 is a dual-specificity kinase capable of phosphorylating serine, threonine, and tyrosine residues (Hoekstra et al., 1994). Since budding yeast lack kinases that specifically target tyrosine residues, phosphorylation is mediated by dual-specificity kinases like HRR25. Given that the kinase responsible for phosphorylating γ-tubulin Y445 remains unknown, the detection of HRR25 implicates it as a candidate. While information regarding the consensus motif for HRR25 tyrosine phosphorylation is incomplete, it has been reported that negatively charged residues adjacent to the tyrosine likely play a role in its recognition of substrates, a characteristic found in the highly negatively charged γCT.

Lastly, novel interactions with the proteins ESL1 and ESL2 were detected, with ESL1 having been detected in both experiments. Information on ESL1 or its paralog ESL2 in the literature is very sparse, however, one study has implicated them in adaptive gene responses carried out

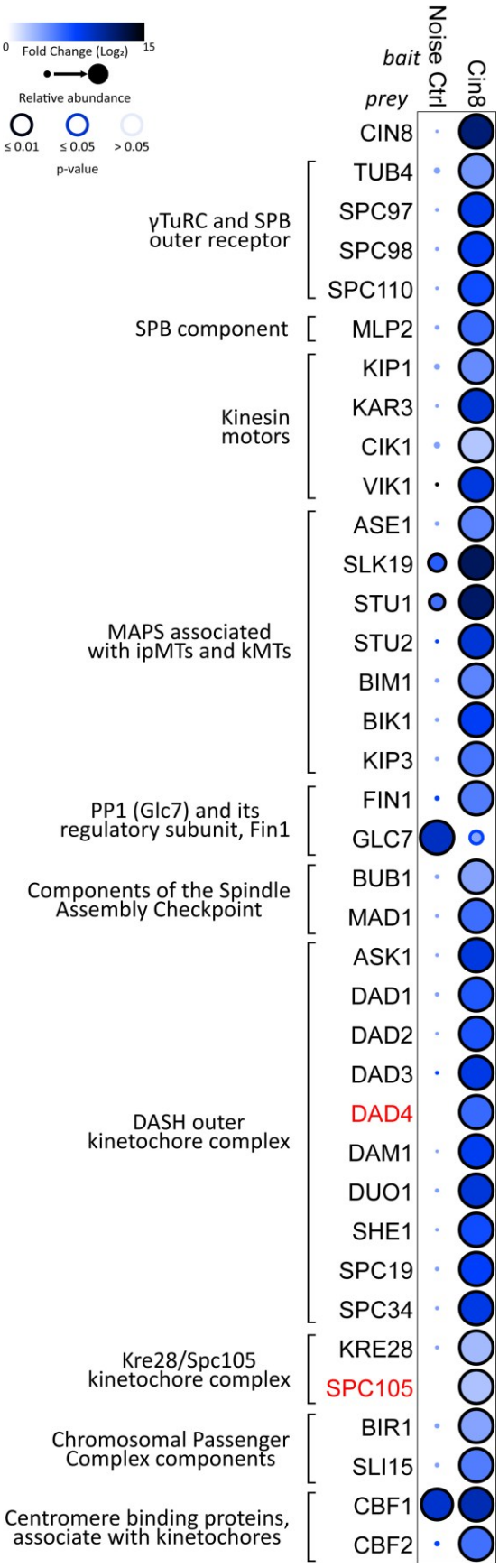

Figure 3.11. Curated proteins identified using a Cin8 bait with yeast-optimized TurboID. Select interactors identified in the Cin8-TurboID screen are shown in a dot plot. The class of each protein is indicated to the left of the identified (or prey) protein names. The relative enrichment of protein signals, comparing the Cin8 bait and a noise control (mNeonGreen-TurboID) against a background control (no TurboID enzyme), is displayed on a log2 scale. Prey proteins highlighted in black were identified in ≥2 separate experiments; proteins highlighted in red were identified in one experiment. The size of the circle in each row reflects the relative abundance of the protein within the strain corresponding to each column.

within environmental sensing pathways (Lai et al., 2013). As well, interestingly, ESL1 and ESL2 have been shown to physically interact with HRR25, though the function behind this interaction is unclear (Dehecq et al., 2018; Lai et al., 2013; Michaelis et al., 2023).

3.3.1. Cin8 interacts with key complexes involved in spindle dynamics and diverse cellular pathways.

Compared to the Spc97 experiment, Cin8-TurboID identified a significantly greater number of proteins involved in various cellular pathways, possibly due to Cin8's broader pattern of localization within the spindle apparatus, including the SPBs, along MTs, and at kinetochores (Figure 2.11). Of note, Cin8-TurboID identified interactions with Kip1—the other budding yeast kinesin-5—and Ase1, supporting the previous report of Cin8 directly interacting with Ase1. However, interactions with Cdc28—or mitotic cyclins—was not detected in

either γ-tubulin WT or Y445D backgrounds. This is likely due to the limitation of MS in detecting proteins with a low number of residues, like Cdc28 and cyclins, which produce very few peptides. Additionally, interactions with other spindle and midzone proteins were detected, including Kar3, Vik1, Bim1, Stu1, Stu2, Kip3 and Slk19. As well, interactions were detected with Fin1—similar to Spc97-TurboID—and Bik1.

Fin1 is a regulatory subunit of Protein Phosphatase 1 (PP1) that localizes to the spindle and kinetochores, but only after dephosphorylation by Cdc14 during anaphase (Sherwin & Wang, 2019). Although the specific function of the Fin1-PP1 complex on the spindle and kinetochores remains unclear, it has been shown to silence the SAC by promoting the removal of SAC proteins Bub1 and Bub3 (Bokros et al., 2016, 2021). The functional significance of an interaction between Cin8 and Fin1 is unclear. However, Suzuki et al. (2018) demonstrated that PP1 co-purifies with Cin8, indicating a direct interaction between these proteins. Their study further suggested that Cin8 mediates the recruitment of PP1 to kinetochores through a conserved PP1-binding motif (RVKW) located within an unstructured region of Cin8. Mutation of this motif significantly reduced the amount of PP1 co-purified with both Cin8 and the kinetochore protein Dsn1. However, this finding requires further replication and validation, and whether it involves Fin1 remains to be determined.

Bik1, the yeast ortholog of CLIP-170, is a MT +TIP that exists in both cytoplasmic and nuclear pools (Berlin et al., 1990; Julner et al., 2022). The cytoplasmic pool contributes to spindle positioning, but less is known regarding the function of the nuclear pool. However, Julner et al. (2022) demonstrated that nuclear Bik1 localizes to kinetochores during metaphase, playing a critical role in kinetochore positioning and chromosome congression. Forcing the nuclear export of Bik1 caused delays in the metaphase-to-anaphase transition and resulted in defects in chromosome biorientation. Using a TurboID proximity-labeling method—relying on western blot analysis instead of MS—they identified interactions between Bik1 and both yeast kinesin-5 proteins, Kip1 and Cin8. Importantly, deleting Cin8 significantly reduced the amount of Bik1 on the spindle, suggesting that Cin8 is crucial for Bik1's spindle association. The consistent identification of Bik1 in the Cin8-TurboID pulldown further supports its interaction with Cin8.

To further explore these interactions and the ability of this method to preserve native protein complexes, I queried the STRING database, a comprehensive repository of known and predicted protein-protein interactions (Szklarczyk et al., 2019), using the Cin8 dataset. I extracted protein interactions—filtering for only experimentally determined physical interactions—with a STRING confidence score greater than 0.9, representing these proteins as nodes and their interactions as edges in the network. Furthermore, I queried the APID (Agile Protein Interactomes DataServer) database, which integrates known experimentally validated protein-protein interactions, using a confidence score of ≥ 1 experimental evidence. To better understand the functional organization of these interactions, I applied the Markov cluster algorithm (Van Dongen, 2008) individually to the interactions derived from the two databases, to identify distinct clusters of interconnected nodes and subsequently analyzed the genes within each cluster to determine their potential roles in cellular processes (Figure 2.12 and Figure 2.13).

This analysis revealed several clusters corresponding to distinct functional cellular complexes, including a cluster corresponding to the three γTuRC components—Spc97, Spc98, and γ-tubulin—with Spc110, the DASH outer kinetochore complex, and the anaphase promoting complex. Additionally, a cluster of proteins involved in controlling spindle assembly, stability, and elongation was identified, with several proteins overlapping those found in the Spc97-TurboID screen. Several large complexes, such as the spliceosomal complex and proteins involved in DNA replication and repair, were also detected. While these complexes were not enriched in the noise control, it remains unclear whether Cin8 directly participates in these pathways or if these proteins co-purified with another Cin8 interactor. For example, the Cin8-TurboID screen also identified the centromeric binding proteins CBF1 and CBF2 (Ndc10), the former of which also binds non-centromeric sites. These, or other identified proteins which localize to centromeres and bind DNA, could potentially co-purify chromatin-related proteins. However, several of the enriched complexes represent normal cellular functions, such as Cin8 synthesis (preribosome, large subunit) or targeted degradation during mitosis (APC).

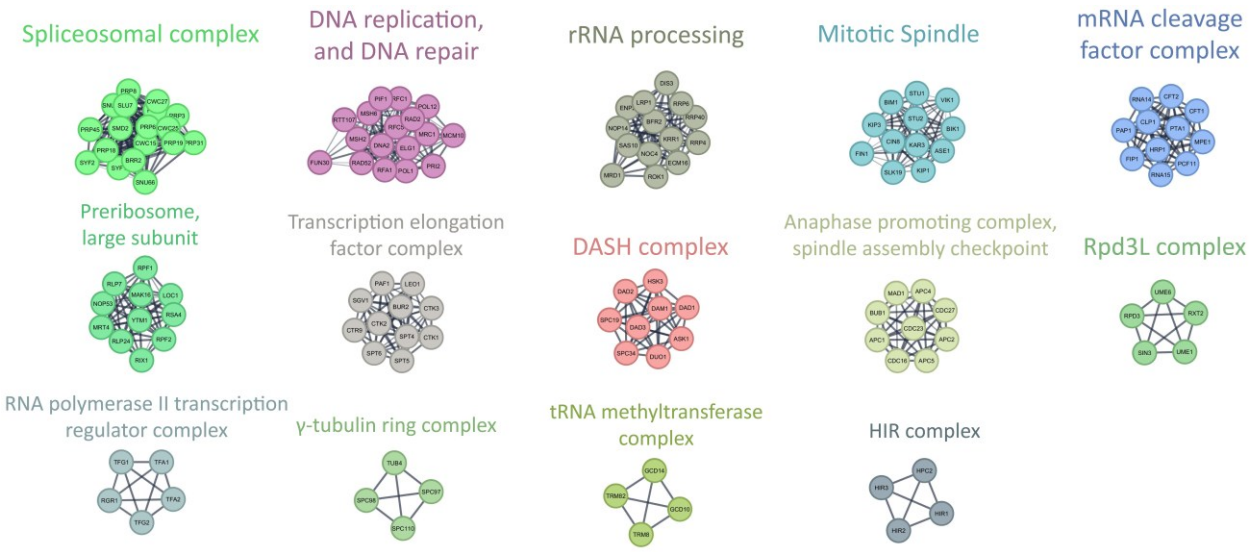

Figure 3.12. Clustering of Cin8 interactions identify key complexes involved in spindle dynamics and diverse cellular pathways (using STRING database). Proteins significantly identified in ≥2 Cin8-TurboID datasets were used to query the STRING database for physical interactions reported in the literature, with a confidence score threshold of ≥ 0.9. The interconnected proteins (nodes) and their interactions (edges) extracted from STRING were clustered using the Markov clustering algorithm, and the genes within each cluster were analyzed. Each cluster was labeled according to the corresponding complex or cellular pathway it represents, providing insights into the functional relationships between the identified proteins.

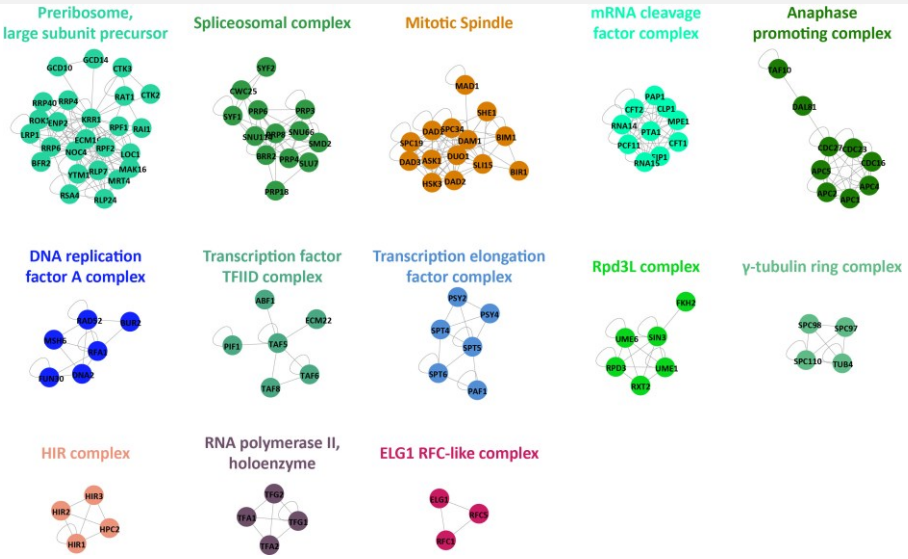

Figure 3.13. Clustering of Cin8 interactions identify key complexes involved in spindle dynamics and diverse cellular pathways (using APID database). Proteins significantly identified in ≥2 Cin8-TurboID datasets were used to query the APID database for physical interactions reported in the literature, with a confidence score threshold of ≥ 1 experimental evidence. The interconnected proteins (nodes) and their interactions (edges) extracted from APID were clustered using the Markov clustering algorithm, and the genes within each cluster were analyzed. Each cluster was labeled according to the corresponding complex or cellular pathway it represents, providing insights into the functional relationships between the identified proteins.

3.3.2. Impact of the γ-tubulin Y445D mutation on the Cin8 interactome.

The most striking finding was the significant decrease in all γTuRC proteins in the presence of the Y445D mutation, with $\log_2$ fold-changes of -2.18, -3.31, and -2.01 for Spc97, Spc98, and Tub4, respectively (Figure 2.13 and Table 3.1). There are two potential explanations for this result. First, the Y445D mutation may destabilize the interaction between γ-tubulin and Cin8, reducing the signal of the γTuRC proteins. Second, the Y445D mutation could result in Cin8 being sequestered in a location outside the labeling radius of TurboID. In the Y445D mutant, Cin8 is sequestered near the older SPB, but the precise binding location remains unclear. Evidence indicates an increased number of MTs in Y445D cells, and since Cin8 can crosslink parallel MTs, it is possible that the Y445D mutation leads to Cin8 being sequestered on parallel bundles of MTs. This sequestration could result in the decreased signal for the γTuRC detected in the Y445D background.

UniProt ID	Gene Name	Protein Name	Fold-change	p-value
Q12107	APC9	Anaphase-promoting complex subunit 9	-4.76	2.86E-04
P47134	BIR1	Protein BIR1	-4.17	5.44E-04
P53540	SPC98	Spindle pole body component SPC98	-3.31	2.69E-04
P14724	CDC26	Anaphase-promoting complex subunit CDC26	-2.63	1.89E-02
Q04431	KRE28	Spindle pole body component KRE28	-2.61	1.51E-02
Q02629	NUP100	Nucleoporin NUP100/NSP100	-2.61	1.41E-02
P53148	SPC105	Spindle pole body component SPC105	-2.34	6.74E-04
P38863	SPC97	Spindle pole body component SPC97	-2.18	1.84E-03
P53378	TUB4	Tubulin gamma chain	-2.01	2.39E-05

Table 3.1. The Y445D mutation reduces the Cin8-TurboID detection of the γTuRC and other spindle proteins. Proteins determined to have significantly reduced signal in a Cin8-TurboID strain with the Y445D mutation are listed. To determine significant decreases only proteins which were significantly enriched in a γ-tubulin WT strain were examined, and a $\log_2$ fold-change (γ-tubulin Y445D/WT) threshold of ≤ -2.0 and an adjusted p-value of 0.05 was used.

In addition to the γTuRC, the Y445D mutation correlated with a substantial reduction in the kinetochore proteins Spc105, Kre28, and Bir1, with $\log_2$ fold-changes of -2.34, -2.61, and -4.17, respectively. Spc105 and Kre28 are known to localize to kinetochores and form a complex essential for the binding of several kinetochore MAPs, including Bim1, Bik1, Slk19, as well as Cin8 and Kar3 (Roy et al., 2022). Similarly, Bir1 localizes to the kinetochores as a component of the chromosomal passenger complex (Sherwin & Wang, 2019), where it contributes to chromosome

biorientation and SAC activation. The identification of Spc105 and Kre28—and potentially Bir1—in γ-tubulin WT cells could be linked to Cin8's function as a length-dependent kMT depolymerase, as Cin8 is known to localize to kMTs and move toward the plus-end, contributing to kMT length regulation during kinetochore search-and-capture (Gardner et al., 2008).

Given that Cin8 appears sequestered near the old SPB in Y445D cells, the reduced signal of kinetochore-localized proteins could be due to a localization defect that limits Cin8's access to other regions of the cell. This restricted access could also explain the reduced signal for the nucleoporin Nup100, which is localized within the nuclear pore complex. Lastly, a reduction in signal for the anaphase promoting complex components Apc9 and Cdc26 was detected, potentially indicating a reduced ability for the anaphase promoting complex to access Cin8 for targeted degradation. Conversely, many new interactions enriched for proteins involved in cell wall organization were detected by Cin8-TurboID in the γ-tubulin Y445D background. This observation could potentially be explained by the sequestration of Cin8 to parallel bundles of MTs originating from the old SPB. During budding yeast cell division, the older SPB migrates into the daughter cell (also called the bud; Pereira, 2001). As the old SPB passes through the bud neck—the constriction between the mother and daughter cells—a high concentration of Cin8-TurboID localized near the old SPB on MT bundles could become proximal to the membrane, resulting in biotinylation of membrane proteins and co-purification of cell wall proteins. Additionally, the Y445D mutation produces a metaphase delay, which likely results in an increase in the overall signal of metaphase proteins.

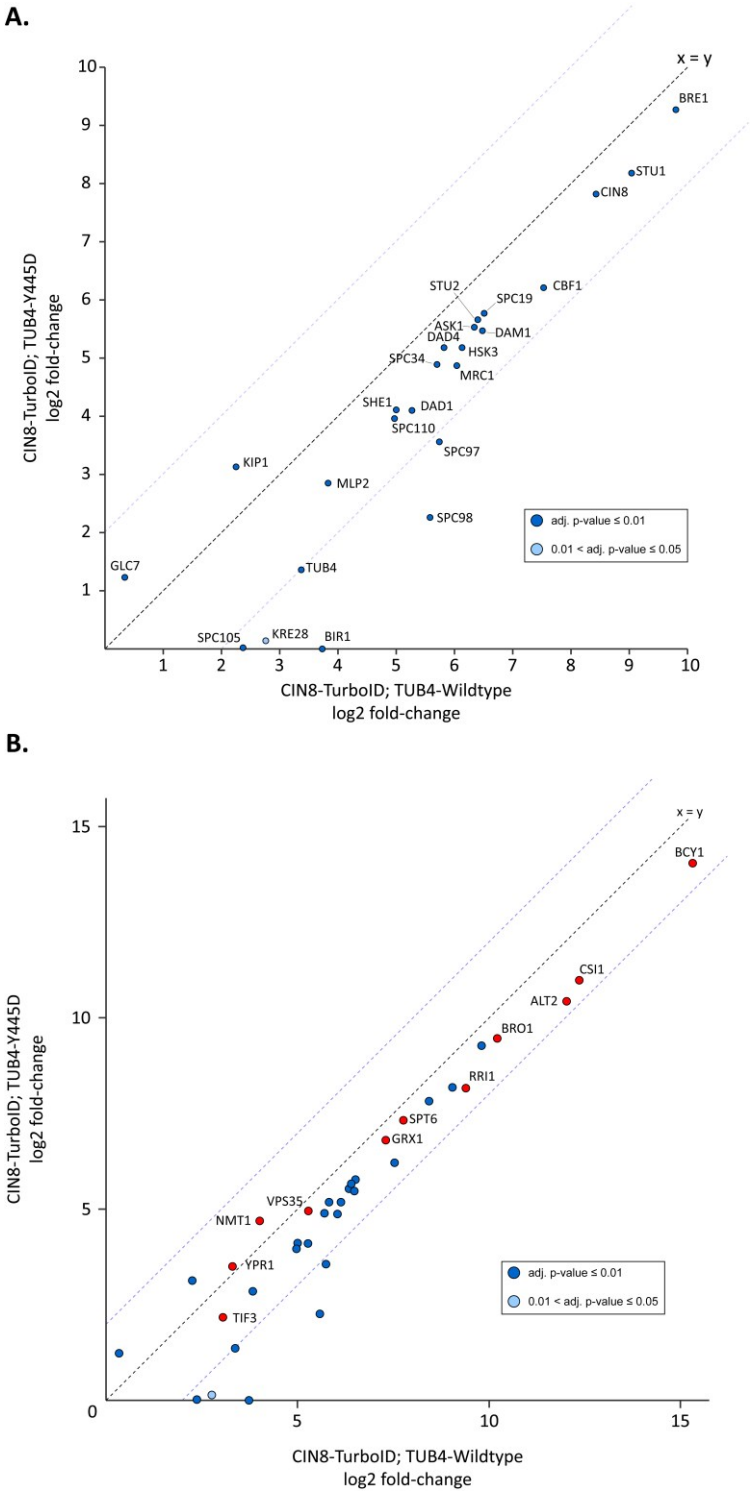

Figure 3.14. The Y445D mutation inhibits Cin8 interactions with γTuRC and kinetochore proteins. (A) The $\log_2$ enrichment of high-confidence prey proteins detected using Cin8-TurboID in both γ-tubulin WT (x-axis) and Y445D (y-axis) backgrounds is shown. **(B)** The same plot as in **(A)**, but with noise control hits included. Noise control hits with mitotic spindle functions were filtered out to prevent any bias caused by the Y445D mutation affecting these proteins.

CHAPTER 4 – DISCUSSION AND FUTURE DIRECTIONS

In this study, I adapted a yeast-optimized BioID protocol to investigate γ-tubulin interactions, focusing specifically on how the γ-tubulin Y445D mutation influences the interactome of the budding yeast kinesin-5 Cin8. Building upon the method published by Fenech et al. (2023), which enabled the efficient reduction of native enzyme biotinylation that can mask BioID detection of interactors in yeast, I incorporated several important modifications. These included yeast cryo-grinding coupled with mild denaturation conditions to preserve transient interactions and native protein complexes; chemical treatment of streptavidin-conjugated agarose to prevent proteolytic digestion of streptavidin and subsequent MS contamination; and the introduction of the newer AID2 technology to improve the reduction of native biotinylation, particularly of Acc1, the most abundant biotinylated enzyme.

Using this optimized method, I screened for interactors of Spc97—a γTuRC component stably associated with γ-tubulin—and of Cin8. For both protein baits, I detected a network of proteins involved in spindle stability, assembly, and elongation. Many of these proteins are known to localize to either the spindle poles or the midzone; however, for several of them, this represents the first detection of physical interactions with Spc97 and Cin8. Importantly, I also provide evidence supporting the interaction of Cin8 with the γTuRC in WT cells and observed that the Y445D mutation appears to inhibit this interaction.

4.1. TurboID provides evidence for an interaction between Cin8 and γ-tubulin.

Using yeast-optimized TurboID, I identified all three γTuRC proteins—Spc97, Spc98, and γ-tubulin—as well as the nuclear receptor Spc110 in the Cin8 bait strain, supporting an interaction between Cin8 and the γTuRC. However, in the reciprocal experiment using Spc97-TurboID as bait, I was unable to detect Cin8. This discrepancy could be due to several factors. One possibility is that the stoichiometry of the interaction decreases the detection signal of Cin8 in the Spc97 bait strain, given that there are four Cin8 molecules in the homotetramer and seven Spc97 molecules in the γTuRC. However, two more likely explanations involve technical limitations of MS analysis.

First, detecting proteins present at significantly lower concentrations relative to others in a sample is a common challenge in MS. Low-abundance proteins generate weaker signals, which

can be masked by the more intense signals from higher-abundance proteins such as Acc1. Cin8 has significantly lower cellular abundance compared to Spc97, Spc98, and γ-tubulin, with a median of 763 ± 682 Cin8 molecules per cell, compared to median abundances of 1794 ± 378 Spc97, 1528 ± 710 Spc98, and 3148 ± 1751 γ-tubulin molecules per cell (as reported on SGD). Additionally, Cin8 has a much shorter half-life, measured by Christiano et al. (2014) to be 1.3 hours, compared to the 11.3-hour half-life of Spc98 (the half-lives of Spc97 and γ-tubulin were not measured in this study). This means that biotinylated Cin8 molecules are likely degraded faster relative to γTuRC proteins. As a result, there would be a decreased pool of biotinylated Cin8 in the Spc97 bait strain, making detection more difficult using MS.

However, these issues could likely be overcome in future experiments by optimizing several aspects of the method. For example, alternative proteases could be tested, the chromatographic gradient could be lengthened to improve protein separation, or potentially high abundant proteins (such as Acc1) could be depleted before the purification of biotinylated proteins. Alternatively, to confirm the presence of specific candidate interactions—such as Cin8—a protein tag could be fused to the protein of interest, which could then be detected on western blot after the biotin labeling and subsequent streptavidin purification.

4.2. The γ-tubulin Y445D mutation inhibits the detection of γTuRC proteins by Cin8-TurboID

Our lab's previous work has indicated that in Y445D cells, Cin8 becomes sequestered near the older SPB, but the exact mechanism remains unknown. A goal of my project was to investigate proteins that interact with either Spc97 or Cin8 and to determine whether the Y445D mutation influences these interactions. This could reveal whether the γCT in Y445D cells directly recruits Cin8 or inhibits its release from the minus-end, or if it perturbs the normal regulation of Cin8. However, due to the synthetic lethality of the Spc97-TurboID and γ-tubulin Y445D combination, I was limited to investigating the influence of Y445D in the Cin8-TurboID bait strain.

Despite this limitation, my work provides evidence that Cin8 interacts with the γTuRC and suggests that this interaction is inhibited to some degree in Y445D cells. If this is the case, two possibilities arise. The first is that the Y445D mutation destabilizes the γTuRC or the MT minus-end, either resulting in a decrease in the number of γTuRCs or an inhibition of γTuRC interactions

with Cin8. However, prior evidence has indicated that γ-tubulin Y445D protein is expressed at levels similar to the WT protein (Vogel et al., 2001). Additionally, γTuRCs containing the Y445D mutation can be purified at similar levels to those with the WT γ-tubulin (unpublished), suggesting that the mutation does not significantly affect the overall expression or assembly of the ring complexes.

An alternate possibility is the Y445D mutation may disrupt the phosphorylation of Cin8, which is normally mediated by Cdc28 (CDK1) during mitosis (Khmelinskii et al., 2009; Avunie-Masala et al., 2011). This phosphorylation event reduces Cin8's affinity for MTs and plays a crucial role in regulating its localization (Goldstein et al., 2017). Inhibiting this phosphorylation could increase Cin8's MT-binding affinity, potentially trapping it on parallel MT bundles near the older SPB before the newer SPB nucleates MTs. This hypothesis aligns with the observation that Cin8 sequestration at the older SPB is exacerbated in Y445D cells expressing the phospho-inhibited Cin8-3A mutant, further supporting the idea that Y445D disrupts Cin8's phosphoregulation. Furthermore, Y445D cells appear to have more MTs, which could increase the chance for Cin8 to encounter and crosslink adjacent parallel MTs. In this location, the γTuRC would likely be outside the labeling range of Cin8-TurboID, resulting in decreased signal detection. Future work could focus on either characterizing the number of γTuRCs in Y445D cells or investigating the localization of Cin8 sequestered near the old SPB at greater resolutions. The former could provide information on the stability of the γTuRC in Y445D cells, while the latter could potentially verify if Cin8 becomes stuck on parallel bundles of MTs close to the SPB.

4.3. Cin8-TurboID labeling of kinetochore-associated proteins and the nucleoporin Nup100 is decreased in Y445D cells.

Apart from the γTuRC proteins and Spc110, the Y445D mutation appeared to decrease the Cin8-TurboID signal of proteins associated with kinetochores—specifically Spc105, Kre28, and Bir1—as well as the nucleoporin Nup100. This decrease could potentially be explained by the sequestration of Cin8 in Y445D cells, which may limit the access of Cin8-TurboID to other parts of the cell, including the kinetochores—since Cin8 is known to localize to the plus-ends of kinetochore microtubules (kMTs)—and the nuclear pore complex. Interestingly, I did not observe

significant reductions in other spindle proteins, and as previously mentioned, I could not detect Cdc28. Therefore, it remains unclear whether the Y445D mutation perturbs the phosphoregulation of Cin8.

However, a significant issue with the experimental design likely limited the detection of changes in Cin8's interactome. The Y445D mutation has been shown to activate the SAC and delay the transition to anaphase, effectively increasing the time Y445D cells spend in metaphase (Shulist et al., 2017; Vogel et al., 2001). Consequently, during the TurboID labeling experiment, the cell cycle distribution of Y445D cells would be biased toward metaphase relative to WT cells. This bias would result in an enrichment of metaphase-specific proteins in the Y445D fraction of biotinylated proteins—particularly midzone and other spindle proteins—leading to an artificial increase in their signal relative to WT cells. As many spindle proteins in Y445D cells exhibited $\log_2$ fold-changes between 1 and 2, it is possible that correcting for this cell cycle bias could reveal that these proteins are also significantly decreased in Y445D cells.

4.4. Identification of literature-reported interactions by yeast TurboID.

TurboID has proven to be an effective tool for detecting native protein interactions in budding yeast. The quality of a reported protein-protein interaction is often assessed by the number of experimental sources supporting it. Compared to the BioGrid database, the Spc97-TurboID screen identified five of the six γ-tubulin interactors with strong supporting evidence (>1 publication), including Spc72, Spc97, Spc98, Spc110, and Stu2, though it missed Pfk1. Additionally, the screen revealed five other interactors—Kar3, Cmd1, Hrr25, Cmk2, and Mlp2—that had previously been reported with limited evidence (one publication each). In contrast, there is limited information available on physical interactions involving Cin8. Nevertheless, the Cin8-TurboID screen detected several physical interactions with limited prior physical evidence, notably identifying Ase1, a midzone crosslinker reported to interact directly with Cin8 to facilitate its midzone recruitment (Khmelinskii et al., 2009).

Several factors may account for why certain protein interactions reported in the literature were not detected by either bait strain. In part, technical experimental issues could be a potential explanation specific to the Spc97-TurboID bait experiment. Consistently, after proteolytic

digestion of the biotinylated proteins corresponding to the Spc97-TurboID strain, the peptide samples became macroscopically viscous with a gel-like consistency. The sample consistency was reminiscent of the gel-like consistency of γCT purifications at low pH which were previously reported in Payliss et al. (2019). This resulted in a dramatic reduction of NMR peak intensities, which was hypothesized to potentially arise from the purified γCTs formed a system spanning network invisible to solution NMR.

UniProt ID	Gene Name	Protein Name	Experimental Evidences	BgCtrl	mNG-Ctrl	Cin8-TurboID	Spc97-TurboID
P16861	PFK1	ATP-dependent 6-phosphofructokinase subunit alpha	4	56	56	56	29
P00546	CDC28	Cyclin-dependent kinase 1	2	4	5	3	0
P10592	SSA2	Heat shock protein SSA2	2	45	46	48	27
P10591	SSA1	Heat shock protein SSA1	1	45	45	47	25
P11484	SSB1	Heat shock protein SSB1	1	34	35	34	19
P15108	HSC82	ATP-dependent molecular chaperone HSC82	1	41	41	39	22
P25491	YDJ1	Mitochondrial protein import protein MAS5	1	16	16	16	10
P25694	CDC48	Cell division control protein 48	1	29	29	29	18
P32589	SSE1	Heat shock protein homolog SSE1	1	26	27	29	19

Table 4.1. Kinases and heat shock proteins reported to interact with γ-tubulin are potential natively biotinylated proteins. This table lists kinases and heat shock proteins previously reported as γ-tubulin interactors in the APID interaction database, which compiles data from BioGrid, IntAct, and DIP. These proteins, potentially natively biotinylated, did not show significant enrichment in Spc97-TurboID samples. The table includes an " Experimental Evidences" column, providing a metric for interaction reliability based on replication frequency, and details the total peptides detected for each protein across all conditions.

During MS analysis of the purified biotinylated proteins, the Spc97-TurboID samples caused increased back pressure and clogging in the chromatography column, likely due to high sample viscosity. This issue reduced MS sensitivity and consequently decreased the detection of peptides, including background proteins that typically remain consistent across samples (see Table 4.1). I hypothesize that this reduced MS sensitivity may have impaired the detection of the literature reported interacting proteins. The Spc97-TurboID biotinylated peptides would contain a greater number of peptides derived from γ-tubulin (including γCT peptides) relative to the other baits, so the source of the increased viscosity of γCT purifications in Payliss et al. (2019) could be producing similar effects in the present samples and leading to reduced MS sensitivity. Future experiments should address this viscosity issue by testing different experimental conditions used for the protein purification or column chromatography. For example, the pH or salt concentrations of final purification and wash buffers could be adjusted, the cleaning and drying of the peptides

could be further optimized, or alternate chromatography columns or gradient lengths could be used.

Another potential explanation is the presence of native biotinylation, which can interfere with BioID detection. For instance, Pfk1, a key metabolic regulator, showed a similar peptide count across all samples (Table 4.1), suggesting that it may already be biotinylated *in vivo*. Given the strength of the biotin-streptavidin interaction, TurboID labeling of a natively biotinylated protein likely would not significantly increase its signal relative to WT cell lysates. A possible solution would be to purify biotinylated proteins using a modified version of Streptavidin with less affinity for biotin, or an anti-biotin antibody, which would allow efficient elution of biotinylated peptides. As biotinylated peptides remain on the agarose beads after proteolytic digestion, the ability to elute these would enable detection of specific residues biotinylated by TurboID (for an example, see D. I. Kim et al., 2018). The identification of biotinylated residues in bait strains—that are not observed in controls—could improve the ability to identify interactors using TurboID, or perhaps provide structural context for an interaction when overlaid on the proteins structure.

4.5. TurboID identifies potential novel interactors of Spc97 and Cin8.

In addition to previously documented interactions, yeast-optimized TurboID enabled the detection of potentially novel interactions for both Spc97 and Cin8. The Spc97-TurboID screen identified Hrr25, corroborating prior reports of interactions between γ-tubulin and this kinase. It also detected Fin, a PP1 regulatory subunit, along with the poorly characterized paralogs ESL1 and ESL2. Given the rarity of Y445 phosphorylation, we hypothesize it may be a stress-induced event, aligning with the observed environmental adaptivity functions of ESL1 and ESL2. Additionally, both ESL1 and ESL2 are reported Hrr25 interactors. This raises the possibility that an environmental cue could target a complex of ESL1, ESL2, and Hrr25 to regulate Y445 phosphorylation. However, the hypothesis that Y445 phosphorylation could be environmentally regulated remains highly speculative. The proposed link to ESL1 and ESL2, in particular, is uncertain due to the limited data on these proteins. While ESL1 and ESL2 roles in environmental sensing pathways are suggestive, further investigation would be required to establish any

relationship with Y445 phosphorylation. For example, future experiments could utilize other methods of detecting protein interactions to validate a potential interaction between Spc97/γ-tubulin and ESL1 or ESL2, such as co-immunoprecipitation or solution NMR experiments.

The screen also identified two additional interactors, Bre1 (an E3 ubiquitin ligase involved in histone regulation) and its binding partner Lge1 (W. W. Hwang et al., 2003; J. Kim et al., 2018). Despite their canonical functions in gene regulation, these proteins were consistently enriched over controls in both Spc97- and Cin8-TurboID screens. Interestingly, the Vogel lab's 2017 high-throughput screen showed that deleting Bre1 or Lge1 is synthetically lethal with the Y445D mutation (Shulist et al., 2017), and recent structural studies of the budding yeast γTuRC identified an enrichment of Bre1 at SPBs (Dendooven et al., 2024). Moreover, in breast cancer cell lines, Duan et al. (2016) demonstrated that the Bre1 homolog complex, RNF20/40, monoubiquitinates and stabilizes Eg5 (a Cin8 homolog), with loss of RNF20/40 leading to spindle assembly defects. However, this study requires experimental replication, and it remains uncertain whether this function would translate effectively to budding yeast or to non-cancerous cell lines.

Conclusion

The fidelity of chromosome segregation relies on the precise coordination of hundreds of proteins to organize and bundle MTs into specialized arrays aligned with cell cycle events. Despite this complexity, the mechanisms by which cells regulate individual MT dynamics remain poorly understood. This study aimed to explore a possible mechanism wherein γ-tubulin, the canonical MT nucleator, contributes to assembling the midzone-stabilizing bundle of ipMTs. Research spanning decades in the Vogel lab has connected the phosphorylation of a conserved tyrosine residue, Y445, in the γCT to spindle assembly, with the phospho-mimetic Y445D mutation activating the SAC and delaying the transition to anaphase.

More recently, our lab showed that Y445D disrupts Cin8 function—a kinesin-5 motor critical for midzone and ipMT formation—leading to nascent bipolar spindle instability (Sim et al., 2024). However, the γCT's role in ipMT formation has remained unclear, largely due to the lack of identified interacting proteins. Given the hypothesis that γ-tubulin interactions beyond the MTOC might be transient or low-affinity, we adapted TurboID, a proximity-labeling technique, to detect

such interactions. Although seldom used in budding yeast due to native biotinylation of endogenous enzymes, we optimized TurboID to 1) preserve transient interactions and native protein complexes using cryo-grinding and mild denaturation, and 2) identify interactors that may be involved in ipMT stabilization and explore their response to the Y445D mutation.

This study demonstrates that TurboID is effective for capturing protein interactions in budding yeast. Applied to the Spc97 and Cin8 interactomes, yeast TurboID identified numerous proteins localized to SPBs, spindle MTs, or kinetochores—many not previously recognized as interactors of these baits. Additionally, the study suggests that Cin8 interacts with the γTuRC and that the Y445D mutation disrupts this interaction, a finding previously unknown. Beyond expected interactions, several potential novel interactors were identified for both Spc97 and Cin8, underscoring TurboID's ability to capture elusive interactions that traditional biochemical techniques may overlook.

This work sets the stage for numerous future experiments. Further research could validate the newly identified interactions for Spc97 and Cin8 and assess if these interactors have functions specific to spindle assembly. Specifically, functional assays could be performed to investigate if candidate interactors bind MTs or mitotic proteins. Using the validated interactions, more robust protein interaction networks could be generated and compared to known interactions in both budding yeast and other eukaryotes. Potentially, predicted interactions generated from the MCL clustering of protein interactions could also be experimentally tested/validated. Moreover, upcoming experiments using high-resolution lattice SIM will investigate the stability of the γTuRC in Y445D cells and determine the spatial localization of Cin8 near the older SPB in Y445D cells. Finally, directly probing the functional consequences of Y445D-γTuRC complexes will be essential, as it remains unclear whether Y445D influences γTuRC function or structure in ways not yet understood. Direct confirmation of the structural and functional stability of Y445D-γTuRC complexes would be excellent supporting evidence of γ-tubulin’s role in spindle function. Overally, uncovering why Y445D appears to inhibit Cin8 interactions with the γTuRC will bring us closer to elucidating the molecular mechanisms by which γ-tubulin regulates Cin8 and ipMT assembly.

References

Acuner Ozbabacan, S. E., Engin, H. B., Gursoy, A., & Keskin, O. (2011). Transient protein-protein interactions. *Protein Engineering Design and Selection*, *24*(9), 635–648. https://doi.org/10.1093/protein/gzr025

Akhmanova, A., & Hoogenraad, C. C. (2005). Microtubule plus-end-tracking proteins: Mechanisms and functions. *Current Opinion in Cell Biology*, *17*(1), 47–54. https://doi.org/10.1016/j.ceb.2004.11.001

Akhmanova, A., & Steinmetz, M. O. (2015). Control of microtubule organization and dynamics: Two ends in the limelight. *Nature Reviews Molecular Cell Biology*, *16*(12), 711–726. https://doi.org/10.1038/nrm4084

Aldaz, H., Rice, L. M., Stearns, T., & Agard, D. A. (2005). Insights into microtubule nucleation from the crystal structure of human γ-tubulin. *Nature*, *435*(7041), 523–527. https://doi.org/10.1038/nature03586

Amin, M. A., Agarwal, S., & Varma, D. (2019). Mapping the kinetochore MAP functions required for stabilizing microtubule attachments to chromosomes during metaphase. *Cytoskeleton*, *76*(6), 398–412. https://doi.org/10.1002/cm.21559

Amos, L. A., & Schlieper, D. (2005). Microtubules and Maps. In *Advances in Protein Chemistry* (Vol. 71, pp. 257–298). Elsevier. https://doi.org/10.1016/S0065-3233(04)71007-4

Avunie-Masala, R., Movshovich, N., Nissenkorn, Y., Gerson-Gurwitz, A., Fridman, V., Kõivomägi, M., Loog, M., Hoyt, M. A., Zaritsky, A., & Gheber, L. (2011). Phospho-regulation of kinesin-5 during anaphase spindle elongation. *Journal of Cell Science*, *124*(6), 873–878. https://doi.org/10.1242/jcs.077396

Berlin, V., Styles, C. A., & Fink, G. R. (1990). BIK1, a protein required for microtubule function during mating and mitosis in Saccharomyces cerevisiae, colocalizes with tubulin. *The Journal of Cell Biology*, *111*(6), 2573–2586. https://doi.org/10.1083/jcb.111.6.2573

Bodakuntla, S., Jijumon, A. S., Villablanca, C., Gonzalez-Billault, C., & Janke, C. (2019). Microtubule-Associated Proteins: Structuring the Cytoskeleton. *Trends in Cell Biology*, *29*(10), 804–819. https://doi.org/10.1016/j.tcb.2019.07.004

Bokros, M., Gravenmier, C., Jin, F., Richmond, D., & Wang, Y. (2016). Fin1-PP1 Helps Clear Spindle Assembly Checkpoint Protein Bub1 from Kinetochores in Anaphase. *Cell Reports*, *14*(5), 1074–1085. https://doi.org/10.1016/j.celrep.2016.01.007

Bokros, M., Sherwin, D., Kabbaj, M.-H., & Wang, Y. (2021). Yeast Fin1-PP1 dephosphorylates an Ipl1 substrate, Ndc80, to remove Bub1-Bub3 checkpoint proteins from the kinetochore during anaphase. *PLOS Genetics*, *17*(5), e1009592. https://doi.org/10.1371/journal.pgen.1009592

Branon, T. C., Bosch, J. A., Sanchez, A. D., Udeshi, N. D., Svinkina, T., Carr, S. A., Feldman, J. L., Perrimon, N., & Ting, A. Y. (2018). Efficient proximity labeling in living cells and organisms with TurboID. *Nature Biotechnology*, *36*(9), 880–887. https://doi.org/10.1038/nbt.4201

Brouhard, G. J., & Rice, L. M. (2018). Microtubule dynamics: An interplay of biochemistry and mechanics. *Nature Reviews Molecular Cell Biology*, *19*(7), 451–463. https://doi.org/10.1038/s41580-018-0009-y

Cherry, J. (1998). SGD: Saccharomyces Genome Database. *Nucleic Acids Research*, *26*(1), 73–79. https://doi.org/10.1093/nar/26.1.73

Christiano, R., Nagaraj, N., Fröhlich, F., & Walther, T. C. (2014). Global Proteome Turnover Analyses of the Yeasts S. cerevisiae and S. pombe. *Cell Reports*, *9*(5), 1959–1965. https://doi.org/10.1016/j.celrep.2014.10.065

Daniel Gietz, R., & Woods, R. A. (2002). Transformation of yeast by lithium acetate/single-stranded carrier DNA/polyethylene glycol method. In *Methods in Enzymology* (Vol. 350, pp. 87–96). Elsevier. https://doi.org/10.1016/S0076-6879(02)50957-5

Dehecq, M., Decourty, L., Namane, A., Proux, C., Kanaan, J., Le Hir, H., Jacquier, A., & Saveanu, C. (2018). Nonsense-mediated mRNA decay involves two distinct Upf1-bound complexes. *The EMBO Journal*, *37*(21), e99278. https://doi.org/10.15252/embj.201899278

Dendooven, T., Yatskevich, S., Burt, A., Chen, Z. A., Bellini, D., Rappsilber, J., Kilmartin, J. V., & Barford, D. (2024). Structure of the native γ-tubulin ring complex capping spindle microtubules. *Nature Structural & Molecular Biology*. https://doi.org/10.1038/s41594-024-01281-y

Duan, Y., Huo, D., Gao, J., Wu, H., Ye, Z., Liu, Z., Zhang, K., Shan, L., Zhou, X., Wang, Y., Su, D., Ding, X., Shi, L., Wang, Y., Shang, Y., & Xuan, C. (2016). Ubiquitin ligase RNF20/40 facilitates spindle assembly and promotes breast carcinogenesis through stabilizing motor protein Eg5. *Nature Communications*, *7*(1), 12648. https://doi.org/10.1038/ncomms12648

Dumont, S., & Mitchison, T. J. (2009). Force and Length in the Mitotic Spindle. *Current Biology*, *19*(17), R749–R761. https://doi.org/10.1016/j.cub.2009.07.028

Erickson, H. P. (1995). FtsZ, a prokaryotic homolog of tubulin? *Cell*, *80*(3), 367–370. https://doi.org/10.1016/0092-8674(95)90486-7

Erickson, H. P., & Pantaloni, D. (1981). The role of subunit entropy in cooperative assembly. Nucleation of microtubules and other two-dimensional polymers. *Biophysical Journal*, *34*(2), 293–309. https://doi.org/10.1016/S0006-3495(81)84850-3

Fenech, E. J., Cohen, N., Kupervaser, M., Gazi, Z., & Schuldiner, M. (2023). A toolbox for systematic discovery of stable and transient protein interactors in baker's yeast. *Molecular Systems Biology*, *19*(2), e11084. https://doi.org/10.15252/msb.202211084

Gardner, M. K., Bouck, D. C., Paliulis, L. V., Meehl, J. B., O'Toole, E. T., Haase, J., Soubry, A., Joglekar, A. P., Winey, M., Salmon, E. D., Bloom, K., & Odde, D. J. (2008). Chromosome Congression by Kinesin-5 Motor-Mediated Disassembly of Longer Kinetochore Microtubules. *Cell*, *135*(5), 894–906. https://doi.org/10.1016/j.cell.2008.09.046

Goldstein, A., Siegler, N., Goldman, D., Judah, H., Valk, E., Kõivomägi, M., Loog, M., & Gheber, L. (2017). Three Cdk1 sites in the kinesin-5 Cin8 catalytic domain coordinate motor localization and activity during anaphase. *Cellular and Molecular Life Sciences*, *74*(18), 3395–3412. https://doi.org/10.1007/s00018-017-2523-z

Goodson, H. V., & Jonasson, E. M. (2018). Microtubules and Microtubule-Associated Proteins. *Cold Spring Harbor Perspectives in Biology*, *10*(6), a022608. https://doi.org/10.1101/cshperspect.a022608

Green, N. (1963). AVIDIN. 1. THE USE OF [14C]BIOTIN FOR KINETIC STUDIES AND FOR ASSAY. *Biochemical Journal*, *89*(3), 585–591. https://doi.org/10.1042/bj0890585

Greenlee, M. A., Witt, B., Sabo, J. A., Morris, S. C., & Miller, R. K. (2022). The TOG protein Stu2 is regulated by acetylation. *PLoS Genetics*, *18*(9), e1010358. https://doi.org/10.1371/journal.pgen.1010358

Gudimchuk, N. B., & McIntosh, J. R. (2021). Regulation of microtubule dynamics, mechanics and function through the growing tip. *Nature Reviews Molecular Cell Biology*, *22*(12), 777–795. https://doi.org/10.1038/s41580-021-00399-x

Gunzelmann, J., Rüthnick, D., Lin, T.-C., Zhang, W., Neuner, A., Jäkle, U., & Schiebel, E. (2018). The microtubule polymerase Stu2 promotes oligomerization of the γ-TuSC for cytoplasmic microtubule nucleation. *eLife*, *7*, e39932. https://doi.org/10.7554/eLife.39932

Harris, J., Shadrina, M., Oliver, C., Vogel, J., & Mittermaier, A. (2018). Concerted millisecond timescale dynamics in the intrinsically disordered carboxyl terminus of γ-tubulin induced by mutation of a conserved tyrosine residue: Dynamics of the Gamma Tubulin Carboxy Terminus. *Protein Science*, *27*(2), 531–545. https://doi.org/10.1002/pro.3345

Hildebrandt, E. R., Gheber, L., Kingsbury, T., & Hoyt, M. A. (2006). Homotetrameric Form of Cin8p, a Saccharomyces cerevisiae Kinesin-5 Motor, Is Essential for Its in Vivo Function. *Journal of Biological Chemistry*, *281*(36), 26004–26013. https://doi.org/10.1074/jbc.M604817200

Hoekstra, M. F., Dhillon, N., Carmel, G., DeMaggio, A. J., Lindberg, R. A., Hunter, T., & Kuret, J. (1994). Budding and fission yeast casein kinase I isoforms have dual-specificity protein kinase activity. *Molecular Biology of the Cell*, *5*(8), 877–886. https://doi.org/10.1091/mbc.5.8.877

Hwang, E., Kusch, J., Barral, Y., & Huffaker, T. C. (2003). Spindle orientation in *Saccharomyces cerevisiae* depends on the transport of microtubule ends along polarized actin cables. *The Journal of Cell Biology*, *161*(3), 483–488. https://doi.org/10.1083/jcb.200302030

Hwang, J., & Espenshade, P. J. (2016). Proximity-dependent biotin labelling in yeast using the engineered ascorbate peroxidase APEX2. *Biochemical Journal*, *473*(16), 2463–2469. https://doi.org/10.1042/bcj20160106

Hwang, W. W., Venkatasubrahmanyam, S., Ianculescu, A. G., Tong, A., Boone, C., & Madhani, H. D. (2003). A Conserved RING Finger Protein Required for Histone H2B Monoubiquitination

and Cell Size Control. *Molecular Cell*, *11*(1), 261–266. https://doi.org/10.1016/S1097-2765(02)00826-2

Hyman, A. A., Salser, S., Drechsel, D. N., Unwin, N., & Mitchison, T. J. (1992). Role of GTP hydrolysis in microtubule dynamics: Information from a slowly hydrolyzable analogue, GMPCPP. *Molecular Biology of the Cell*, *3*(10), 1155–1167. https://doi.org/10.1091/mbc.3.10.1155

Janke, C. (2014). The tubulin code: Molecular components, readout mechanisms, and functions. *The Journal of Cell Biology*, *206*(4), 461–472. https://doi.org/10.1083/jcb.201406055

Jaspersen, S. L., & Winey, M. (2004). THE BUDDING YEAST SPINDLE POLE BODY: Structure, Duplication, and Function. *Annual Review of Cell and Developmental Biology*, *20*(1), 1–28. https://doi.org/10.1146/annurev.cellbio.20.022003.114106

Julner, A., Abbasi, M., & Menéndez-Benito, V. (2022). The microtubule plus-end tracking protein Bik1 is required for chromosome congression. *Molecular Biology of the Cell*, *33*(5), br7. https://doi.org/10.1091/mbc.E21-10-0500

Kashlna, A. S., Baskin, R. J., Cole, D. G., Wedaman, K. P., Saxton, W. M., & Scholey, J. M. (1996). A bipolar kinesin. *Nature*, *379*(6562), 270–272. https://doi.org/10.1038/379270a0

Keck, J. M., Jones, M. H., Wong, C. C. L., Binkley, J., Chen, D., Jaspersen, S. L., Holinger, E. P., Xu, T., Niepel, M., Rout, M. P., Vogel, J., Sidow, A., Yates, J. R., & Winey, M. (2011). A cell cycle phosphoproteome of the yeast centrosome. *Science (New York, N.Y.)*, *332*(6037), 1557–1561. https://doi.org/10.1126/science.1205193

Khmelinskii, A., Roostalu, J., Roque, H., Antony, C., & Schiebel, E. (2009). Phosphorylation-Dependent Protein Interactions at the Spindle Midzone Mediate Cell Cycle Regulation of Spindle Elongation. *Developmental Cell*, *17*(2), 244–256. https://doi.org/10.1016/j.devcel.2009.06.011

Kilmartin, J. V. (2014). Lessons from yeast: The spindle pole body and the centrosome. *Philosophical Transactions of the Royal Society B: Biological Sciences*, *369*(1650), 20130456. https://doi.org/10.1098/rstb.2013.0456

Kim, D. I., Cutler, J. A., Na, C. H., Reckel, S., Renuse, S., Madugundu, A. K., Tahir, R., Goldschmidt, H. L., Reddy, K. L., Huganir, R. L., Wu, X., Zachara, N. E., Hantschel, O., & Pandey, A. (2018). BioSITe: A Method for Direct Detection and Quantitation of Site-Specific Biotinylation.

Journal of Proteome Research, *17*(2), 759–769. https://doi.org/10.1021/acs.jproteome.7b00775

Kim, J., An, Y., Park, S., & Lee, J. (2018). Bre1 mediates the ubiquitination of histone H2B by regulating Lge1 stability. *FEBS Letters*, *592*(9), 1565–1574. https://doi.org/10.1002/1873-3468.13049

Kõivomägi, M., Valk, E., Venta, R., Iofik, A., Lepiku, M., Morgan, D. O., & Loog, M. (2011). Dynamics of Cdk1 Substrate Specificity during the Cell Cycle. *Molecular Cell*, *42*(5), 610–623. https://doi.org/10.1016/j.molcel.2011.05.016

Kollman, J. M., Greenberg, C. H., Li, S., Moritz, M., Zelter, A., Fong, K. K., Fernandez, J.-J., Sali, A., Kilmartin, J., Davis, T. N., & Agard, D. A. (2015). Ring closure activates yeast γTuRC for species-specific microtubule nucleation. *Nature Structural & Molecular Biology*, *22*(2), 132–137. https://doi.org/10.1038/nsmb.2953

Kollman, J. M., Merdes, A., Mourey, L., & Agard, D. A. (2011). Microtubule nucleation by γ-tubulin complexes. *Nature Reviews Molecular Cell Biology*, *12*(11), 709–721. https://doi.org/10.1038/nrm3209

Kollman, J. M., Polka, J. K., Zelter, A., Davis, T. N., & Agard, D. A. (2010). Microtubule nucleating γ-TuSC assembles structures with 13-fold microtubule-like symmetry. *Nature*, *466*(7308), 879–882. https://doi.org/10.1038/nature09207

Kristensson, M. A. (2021). The Game of Tubulins. *Cells*, *10*(4), 745. https://doi.org/10.3390/cells10040745

Kuchnir Fygenson, D., Flyvbjerg, H., Sneppen, K., Libchaber, A., & Leibler, S. (1995). Spontaneous nucleation of microtubules. *Physical Review E*, *51*(5), 5058–5063. https://doi.org/10.1103/PhysRevE.51.5058

Kushnirov, V. V. (2000). Rapid and reliable protein extraction from yeast. *Yeast*, *16*(9), 857–860. https://doi.org/10.1002/1097-0061(20000630)16:9<857::AID-YEA561>3.0.CO;2-B

Lai, X., Beilharz, T., Au, W.-C., Hammet, A., Preiss, T., Basrai, M. A., & Heierhorst, J. (2013). Yeast hEST1A/B (SMG5/6)–Like Proteins Contribute to Environment-Sensing Adaptive Gene Expression Responses. *G3 Genes|Genomes|Genetics*, *3*(10), 1649–1659. https://doi.org/10.1534/g3.113.006924

Lakämper, S., & Meyhöfer, E. (2005). The E-Hook of Tubulin Interacts with Kinesin's Head to Increase Processivity and Speed. *Biophysical Journal*, *89*(5), 3223–3234. https://doi.org/10.1529/biophysj.104.057505

Leary, A., Sim, S., Nazarova, E., Shulist, K., Genthial, R., Yang, S. K., Bui, K. H., Francois, P., & Vogel, J. (2019). Successive Kinesin-5 Microtubule Crosslinking and Sliding Promote Fast, Irreversible Formation of a Stereotyped Bipolar Spindle. *Current Biology*, *29*(22), 3825-3837.e3. https://doi.org/10.1016/j.cub.2019.09.030

Lee, R. van der, Buljan, M., Lang, B., Weatheritt, R. J., Daughdrill, G. W., Dunker, A. K., Fuxreiter, M., Gough, J., Gsponer, J., Jones, D. T., Kim, P. M., Kriwacki, R. W., Oldfield, C. J., Pappu, R. V., Tompa, P., Uversky, V. N., Wright, P. E., & Babu, M. M. (2014). Classification of Intrinsically Disordered Regions and Proteins. *Chemical Reviews*, *114*(13), 6589–6631. https://doi.org/10.1021/cr400525m

McKean, P. G., Vaughan, S., & Gull, K. (2001). The extended tubulin superfamily. *Journal of Cell Science*, *114*(15), 2723–2733. https://doi.org/10.1242/jcs.114.15.2723

Meier, S. M., Steinmetz, M. O., & Barral, Y. (2024). Microtubule specialization by +TIP networks: From mechanisms to functional implications. *Trends in Biochemical Sciences*, *49*(4), 318–332. https://doi.org/10.1016/j.tibs.2024.01.005

Menéndez, M., Rivas, G., Díaz, J. F., & Andreu, J. M. (1998). Control of the Structural Stability of the Tubulin Dimer by One High Affinity Bound Magnesium Ion at Nucleotide N-site. *Journal of Biological Chemistry*, *273*(1), 167–176. https://doi.org/10.1074/jbc.273.1.167

Meziane, M., Genthial, R., & Vogel, J. (2021). Kar9 symmetry breaking alone is insufficient to ensure spindle alignment. *Scientific Reports*, *11*(1), 4227. https://doi.org/10.1038/s41598-021-83136-w

Michaelis, A. C., Brunner, A.-D., Zwiebel, M., Meier, F., Strauss, M. T., Bludau, I., & Mann, M. (2023). The social and structural architecture of the yeast protein interactome. *Nature*, *624*(7990), 192–200. https://doi.org/10.1038/s41586-023-06739-5

Mickey, B., & Howard, J. (1995). Rigidity of microtubules is increased by stabilizing agents. *The Journal of Cell Biology*, *130*(4), 909–917. https://doi.org/10.1083/jcb.130.4.909

Müller-Reichert, T., Chrétien, D., Severin, F., & Hyman, A. A. (1998). Structural changes at microtubule ends accompanying GTP hydrolysis: Information from a slowly hydrolyzable analogue of GTP, guanylyl (α,β)methylenediphosphonate. *Proceedings of the National Academy of Sciences*, *95*(7), 3661–3666. https://doi.org/10.1073/pnas.95.7.3661

Musacchio, A. (2015). The Molecular Biology of Spindle Assembly Checkpoint Signaling Dynamics. *Current Biology*, *25*(22), 3017. https://doi.org/10.1016/j.cub.2015.10.050

Nishimura, K., Fukagawa, T., Takisawa, H., Kakimoto, T., & Kanemaki, M. (2009). An auxin-based degron system for the rapid depletion of proteins in nonplant cells. *Nature Methods*, *6*(12), 917–922. https://doi.org/10.1038/nmeth.1401

Nogales, E., Wolf, S. G., & Downing, K. H. (1998). Structure of the αβ tubulin dimer by electron crystallography. *Nature*, *391*(6663), 199–203. https://doi.org/10.1038/34465

Payliss, B. J., Vogel, J., & Mittermaier, A. K. (2019). Side chain electrostatic interactions and pH-dependent expansion of the intrinsically disordered, highly acidic carboxyl-terminus of γ-tubulin. *Protein Science*, *28*(6), 1095–1105. https://doi.org/10.1002/pro.3618

Peng, Y., Moritz, M., Han, X., Giddings, T. H., Lyon, A., Kollman, J., Winey, M., Yates, J., Agard, D. A., Drubin, D. G., & Barnes, G. (2015). Interaction of CK1δ with γTuSC ensures proper microtubule assembly and spindle positioning. *Molecular Biology of the Cell*, *26*(13), 2505–2518. https://doi.org/10.1091/mbc.E14-12-1627

Pereira, G. (2001). Modes of spindle pole body inheritance and segregation of the Bfa1p-Bub2p checkpoint protein complex. *The EMBO Journal*, *20*(22), 6359–6370. https://doi.org/10.1093/emboj/20.22.6359

Peters, J.-M. (2006). The anaphase promoting complex/cyclosome: A machine designed to destroy. *Nature Reviews Molecular Cell Biology*, *7*(9), 644–656. https://doi.org/10.1038/nrm1988

Petry, S. (2016). Mechanisms of Mitotic Spindle Assembly. *Annual Review of Biochemistry*, *85*(1), 659–683. https://doi.org/10.1146/annurev-biochem-060815-014528

Rafiee, M., Sigismondo, G., Kalxdorf, M., Förster, L., Brügger, B., Béthune, J., & Krijgsveld, J. (2020). Protease-resistant streptavidin for interaction proteomics. *Molecular Systems Biology*, *16*(5), e9370. https://doi.org/10.15252/msb.20199370

Ramey, V. H., Wang, H.-W., Nakajima, Y., Wong, A., Liu, J., Drubin, D., Barnes, G., & Nogales, E. (2011). The Dam1 ring binds to the E-hook of tubulin and diffuses along the microtubule. *Molecular Biology of the Cell*, *22*(4), 457–466. https://doi.org/10.1091/mbc.e10-10-0841

Rao, V. S., Srinivas, K., Sujini, G. N., & Kumar, G. N. S. (2014). Protein-Protein Interaction Detection: Methods and Analysis. *International Journal of Proteomics*, *2014*, 1–12. https://doi.org/10.1155/2014/147648

Roll-Mecak, A. (2015). Intrinsically disordered tubulin tails: Complex tuners of microtubule functions? *Seminars in Cell & Developmental Biology*, *37*, 11–19. https://doi.org/10.1016/j.semcdb.2014.09.026

Roostalu, J., Hentrich, C., Bieling, P., Telley, I. A., Schiebel, E., & Surrey, T. (2011). Directional Switching of the Kinesin Cin8 Through Motor Coupling. *Science*, *332*(6025), 94–99. https://doi.org/10.1126/science.1199945

Roostalu, J., & Surrey, T. (2017). Microtubule nucleation: Beyond the template. *Nature Reviews Molecular Cell Biology*, *18*(11), 702–710. https://doi.org/10.1038/nrm.2017.75

Roux, K. J., Kim, D. I., Burke, B., & May, D. G. (2018). BioID: A Screen for Protein-Protein Interactions. *Current Protocols in Protein Science*, *91*(1), 19.23.1-19.23.15. https://doi.org/10.1002/cpps.51

Roux, K. J., Kim, D. I., Raida, M., & Burke, B. (2012). A promiscuous biotin ligase fusion protein identifies proximal and interacting proteins in mammalian cells. *Journal of Cell Biology*, *196*(6), 801–810. https://doi.org/10.1083/jcb.201112098

Roy, B., Sim, J., Han, S. J. Y., & Joglekar, A. P. (2022). Kre28–Spc105 interaction is essential for Spc105 loading at the kinetochore. *Open Biology*, *12*(1), 210274. https://doi.org/10.1098/rsob.210274

Scholey, J. E., Nithianantham, S., Scholey, J. M., & Al-Bassam, J. (2014). Structural basis for the assembly of the mitotic motor Kinesin-5 into bipolar tetramers. *eLife*, *3*, e02217. https://doi.org/10.7554/eLife.02217

Shapira, O., Goldstein, A., Al-Bassam, J., & Gheber, L. (2017). A potential physiological role for bi-directional motility and motor clustering of mitotic kinesin-5 Cin8 in yeast mitosis. *Journal of Cell Science*, *130*(4), 725–734. https://doi.org/10.1242/jcs.195040

She, Z., Wei, Y., Lin, Y., Li, Y., & Lu, M. (2019). Mechanisms of the Ase1/PRC1/MAP65 family in central spindle assembly. *Biological Reviews*, *94*(6), 2033–2048. https://doi.org/10.1111/brv.12547

Sherwin, D., & Wang, Y. (2019). The Opposing Functions of Protein Kinases and Phosphatases in Chromosome Bipolar Attachment. *International Journal of Molecular Sciences*, *20*(24), 6182. https://doi.org/10.3390/ijms20246182

Shulist, K., Yen, E., Kaitna, S., Leary, A., Decterov, A., Gupta, D., & Vogel, J. (2017). Interrogation of γ-tubulin alleles using high-resolution fitness measurements reveals a distinct cytoplasmic function in spindle alignment. *Scientific Reports*, *7*(1), 11398. https://doi.org/10.1038/s41598-017-11789-7

Sim, S., Moore, S., Al-Naemi, K., El-Hajj, Z., & Vogel, J. (2024). Early events in midzone formation stabilize nascent bipolar spindles. *bioRxiv*, 2024.09.09.612135. https://doi.org/10.1101/2024.09.09.612135

Suzuki, A., Gupta, A., Long, S. K., Evans, R., Badger, B. L., Salmon, E. D., Biggins, S., & Bloom, K. (2018). A Kinesin-5, Cin8, Recruits Protein Phosphatase 1 to Kinetochores and Regulates Chromosome Segregation. *Current Biology*, *28*(17), 2697-2704.e3. https://doi.org/10.1016/j.cub.2018.08.038

Szklarczyk, D., Gable, A. L., Lyon, D., Junge, A., Wyder, S., Huerta-Cepas, J., Simonovic, M., Doncheva, N. T., Morris, J. H., Bork, P., Jensen, L. J., & Mering, C. von. (2019). STRING v11: Protein–protein association networks with increased coverage, supporting functional discovery in genome-wide experimental datasets. *Nucleic Acids Research*, *47*(D1), D607–D613. https://doi.org/10.1093/nar/gky1131

Tian, G., Bhamidipati, A., Cowan, N. J., & Lewis, S. A. (1999). Tubulin Folding Cofactors as GTPase-activating Proteins. *Journal of Biological Chemistry*, *274*(34), 24054–24058. https://doi.org/10.1074/jbc.274.34.24054

Van Dongen, S. (2008). Graph Clustering Via a Discrete Uncoupling Process. *SIAM Journal on Matrix Analysis and Applications*, *30*(1), 121–141. https://doi.org/10.1137/040608635

Vogel, J., Drapkin, B., Oomen, J., Beach, D., Bloom, K., & Snyder, M. (2001). Phosphorylation of γ-Tubulin Regulates Microtubule Organization in Budding Yeast. *Developmental Cell*, *1*(5), 621–631. https://doi.org/10.1016/s1534-5807(01)00073-9

Vogel, J., & Snyder, M. (2000). The carboxy terminus of Tub4p is required for γ-tubulin function in budding yeast. *Journal of Cell Science*, *113*(21), 3871–3882. https://doi.org/10.1242/jcs.113.21.3871

Winey, M., & Bloom, K. (2012). Mitotic Spindle Form and Function. *Genetics*, *190*(4), 1197–1224. https://doi.org/10.1534/genetics.111.128710

Yesbolatova, A., Saito, Y., Kitamoto, N., Makino-Itou, H., Ajima, R., Nakano, R., Nakaoka, H., Fukui, K., Gamo, K., Tominari, Y., Takeuchi, H., Saga, Y., Hayashi, K., & Kanemaki, M. T. (2020). The auxin-inducible degron 2 technology provides sharp degradation control in yeast, mammalian cells, and mice. *Nature Communications*, *11*(1), 5701. https://doi.org/10.1038/s41467-020-19532-z